J. Fluid Mech. (2001), *vol.* 439, *pp.* 367–394. Printed in the United Kingdom

Magnetohydrodynamic turbulent flow in a channel at low magnetic Reynolds number

By DONGHOON LEE AND HAECHEON CHOI†

School of Mechanical and Aerospace Engineering, Seoul National University, Seoul 151-742, Korea

(Received 14 March 2000 and in revised form 22 January 2001)

Effects of the Lorentz force on near-wall turbulence structures are investigated using the direct numerical simulation technique with the assumption of no induced magnetic field at low magnetic Reynolds number. A uniform magnetic field is applied in the streamwise (x), wall-normal (y) or spanwise (z) direction to turbulent flow in an infinitely long channel with non-conducting walls. The Lorentz force induced from the magnetic field suppresses the dynamically significant coherent structures near the wall. The skin friction decreases with increasing streamwise and spanwise magnetic fields, whereas it increases owing to the Hartmann effect when the strength of the wall-normal magnetic field exceeds a certain value. All the turbulence intensities and the Reynolds shear stress decrease with the wall-normal and spanwise magnetic fields, but the streamwise velocity fluctuations increase with the streamwise magnetic field although all other turbulence intensities decrease. It is also shown that the wall-normal magnetic field is much more effective than the streamwise and spanwise magnetic fields in reducing turbulent fluctuations and suppressing the near-wall streamwise vorticity, even though the wall-normal magnetic field interacts directly with the mean flow and results in drag increase at strong magnetic fields. In the channel with a strong streamwise magnetic field, two-dimensional streamwise velocity fluctuations $u(y,z)$ exist, even after other components of the velocity fluctuations nearly vanish. In the cases of strong wall-normal and spanwise magnetic fields, all turbulence intensities, the Reynolds shear stress and vorticity fluctuations decrease rapidly and become zero. The turbulence structures are markedly elongated in the direction of the applied magnetic field when it is strong enough. It is shown that this elongation of the structures is associated with a rapid decrease of the Joule dissipation in time.

1. Introduction

The discovery of the change in drag and the suppression of turbulence with an external magnetic field applied to turbulent liquid metal flow is due to Hartmann & Lazarus (1937). Since then, MHD (magnetohydrodynamic) turbulent flow has been an important subject because a static magnetic field alone can suppress turbulent motion in an electrically conducting fluid. Motion of the liquid metal across the magnetic field induces an electric current, which interacts with the magnetic field to generate the Lorentz force. The Lorentz force induced by an external magnetic field not only accelerates decay of the kinetic energy via the Joule dissipation, but also creates an anisotropic eddy structure by elongating the vortices in the direction of the

† Author to whom correspondence should be addressed: e-mail choi@socrates.snu.ac.kr. Also at National CRI center for Turbulence and Flow Control Research, Institute of Advanced Machinery and Design, Seoul National University, Korea.

magnetic field (Alemany *et al.* 1979). A clear understanding of this effect is important, for instance, in the design of liquid metal cooling systems for fusion reactors, in the development of continuous steel-casting processes, in suppressing fluid motion within the mould, and in the development of the technique for growing semiconductor crystals. Moreover, in most MHD flow systems, there exist rigid walls where the Hartmann effect is very important (see below). The present study is aimed at the understanding of the evolution of near-wall turbulence structures when a uniform streamwise, wall-normal or spanwise magnetic field is applied to turbulent flow in an 'infinitely long channel' (hereinafter, simply called a 'channel').

At the beginning of MHD studies, most investigations were carried out experimentally. By measuring velocity profiles in a rectangular channel with wall-normal magnetic fields, Brouillette & Lykoudis (1967) demonstrated the Hartmann effect, which is associated with changes in the mean velocity profile via formation of thin Hartmann layers at insulating boundaries normal to the magnetic field. Fraim & Heiser (1968) showed the turbulence-suppression effect qualitatively in a circular pipe with an axial magnetic field. In a duct flow of liquid metal subject to a wall-normal magnetic field, Reed & Lykoudis (1978) showed that the Reynolds shear stress vanishes with the magnetic field, but the turbulence intensities are still high. In their experiment, the wall-normal magnetic field increased the skin friction by directly altering the mean flow, even though turbulent fluctuations were significantly reduced. On the other hand, a magnetic field in the streamwise or spanwise direction does not directly interact with the mean flow but affects turbulent fluctuations. Therefore, it is possible that such magnetic fields result in drag reduction (Tsinober 1990*a*). However, in liquid metal experiments, it is very difficult to perform flow visualization and accurately measure turbulence quantities, especially in the vicinity of the wall.

In contrast to the numerous experimental studies, there are few theoretical studies on MHD turbulent flow with insulating walls. Sommeria & Moreau (1982) described MHD turbulent flow with a uniform wall-normal magnetic field into two regions: a thin Hartmann layer near the wall and a bulk region of the flow. In the latter region, the elongation process of turbulent eddies along the direction of the magnetic field was considered. They attributed it to the electromagnetic diffusion of vorticity along the magnetic field.

In recent years, direct numerical simulations have emerged as a powerful tool in turbulence structure research. The simulation databases, which contain three-dimensional velocity and pressure fields, provide information to complement experimental data in the study of the physics of turbulent flows. Some interesting features of isotropic turbulence in the presence of a static magnetic field have been found using the direct numerical simulation technique. Oughton, Priest & Matthaeus (1994) investigated a decaying MHD turbulence at large magnetic Reynolds numbers from the full MHD equations, whereas Hossain (1991) and Zikanov & Thess (1998) carried out simulations of forced MHD turbulence at low magnetic Reynolds number. In these studies, it was shown that a sufficiently strong magnetic field is required to suppress turbulent fluctuations in its direction and cause development of anisotropy from initially isotropic flow and eventually a quasi- or purely two-dimensional steady state.

The previous direct numerical simulations of MHD flows have been mostly carried out for isotropic turbulence and, to the best of our knowledge, there were only two numerical studies associated with MHD turbulent flow with non-conducting walls. Shimomura (1991) performed a large-eddy simulation of MHD channel flow under a uniform wall-normal magnetic field and showed that drag increases owing to the Hartmann effect, as observed in the experiment of Reed & Lykoudis (1978). Orlandi

(1996) performed a preliminary direct numerical simulation of turbulent pipe flow with an axial or azimuthal magnetic field using the full MHD equations and showed that some of the experimental observations in liquid metals (Fraim & Heiser 1968; Krasilnikov *et al.* 1971) can be qualitatively described.

The objective of this work is to investigate the effects of the Lorentz force on near-wall turbulence structures using the direct numerical simulation technique with the assumption of no induced magnetic field at low magnetic Reynolds number. A uniform magnetic field is applied in the streamwise, wall-normal or spanwise direction to a turbulent channel flow with non-conducting walls. Different features of MHD flow, in terms of the turbulence statistics as well as instantaneous turbulence structures, according to the direction of the magnetic field are described in detail in this study. Governing equations and numerical methods are given in §§ 2 and 3, respectively. Results of applying uniform magnetic fields in the streamwise, wall-normal and spanwise directions are presented in §§ 4 and 5, followed by a summary in § 6.

2. Governing equations

The governing equations for an electrically conducting and incompressible Newtonian fluid in a channel are written in their non-dimensional forms,

$$\frac{\partial \boldsymbol{u}}{\partial t} + (\boldsymbol{u}\cdot\nabla)\boldsymbol{u} = -\nabla p + \frac{1}{Re}\nabla^2\boldsymbol{u} + N(\boldsymbol{j}\times\boldsymbol{B}), \tag{2.1}$$

$$\frac{\partial \boldsymbol{B}}{\partial t} = \nabla\times(\boldsymbol{u}\times\boldsymbol{B}) + \frac{1}{Re_m}\nabla^2\boldsymbol{B}, \tag{2.2}$$

$$\boldsymbol{j} = \frac{1}{Re_m}\nabla\times\boldsymbol{B}, \tag{2.3}$$

$$\nabla\cdot\boldsymbol{u} = 0, \tag{2.4}$$

$$\nabla\cdot\boldsymbol{B} = 0, \tag{2.5}$$

where $\boldsymbol{u}$ is the velocity, p is the pressure, $\boldsymbol{j}$ is the current density, $\boldsymbol{B}$ is the magnetic field, $Re\,(=\rho U_l\delta/\mu)$, $Re_m\,(=\mu_o\sigma U_l\delta)$, $Al\,(=B^{*2}/\mu_o\rho U_l^2)$ and $N = Re_m Al$ are the Reynolds, magnetic Reynolds, Alfvén and Stuart numbers, respectively, and U_l, δ and B^* denote the characteristic velocity, length and magnetic field, respectively. ρ, σ, μ and μ_o are the density, electrical conductivity, viscosity and magnetic permeability ($=4\pi\times10^{-7}\,\mathrm{H\,m^{-1}}$), respectively. Note that $\boldsymbol{j}$ is normalized in (2.1) and (2.3) such that $\boldsymbol{j} = \boldsymbol{j}^*/\sigma U_l B^*$, where $\boldsymbol{j}^*$ is a dimensional quantity. In these equations, displacement currents, currents arising from charge transport, and forces on concentrations of free charge are neglected (Harris 1960). The Stuart number N is the ratio of the electromagnetic force to the inertial force. The magnetic Reynolds number is the ratio of the induced magnetic field to the applied magnetic field (Branover 1978, p. 19), whereas the Alfvén number is the ratio of the applied magnetic energy to the kinetic energy. Equation (2.1) is the Navier–Stokes equation with the Lorentz force term, and (2.2) is the Maxwell equation which is nonlinearly coupled with (2.1). Note that there are four equations ((2.2) and (2.5)) for three components of the magnetic field $\boldsymbol{B}$, which renders a computational difficulty in satisfying the divergence-free condition (2.5).

In this paper, we consider MHD flow at a low magnetic Reynolds number with a uniform magnetic field. At $Re_m \ll 1$, the induced magnetic field is very small as compared with the applied magnetic field. Therefore, when $Re_m \ll 1$ and the applied

magnetic field does not change in time, $\partial \boldsymbol{B}/\partial t$ can be neglected. With neglecting the induced magnetic field, Ohm's law becomes

$$\boldsymbol{j} = -\nabla\phi + \boldsymbol{u} \times \boldsymbol{B}_o, \tag{2.6}$$

where ϕ is the electric potential ($\boldsymbol{E} = -\nabla\phi$), $\boldsymbol{E}$ is the electric field and $\boldsymbol{B}_o$ is the applied magnetic field which is a unit vector (due to non-dimensionalization) in the streamwise, wall-normal or spanwise direction. Since $\boldsymbol{j}$ is solenoidal, ϕ is determined by taking divergence on (2.6). Thus, in the case of $Re_m \ll 1$ we have the following equations (for the detailed derivation, see Branover 1978):

$$\frac{\partial \boldsymbol{u}}{\partial t} + (\boldsymbol{u}\cdot\nabla)\boldsymbol{u} = -\nabla p + \frac{1}{Re}\nabla^2\boldsymbol{u} + N\{(-\nabla\phi + \boldsymbol{u}\times\boldsymbol{B}_o)\times\boldsymbol{B}_o\}, \tag{2.7}$$

$$\nabla^2\phi = \nabla\cdot(\boldsymbol{u}\times\boldsymbol{B}_o) = \boldsymbol{B}_o\cdot\boldsymbol{\omega}, \tag{2.8}$$

$$\nabla\cdot\boldsymbol{u} = 0, \tag{2.9}$$

where $\boldsymbol{\omega} = \nabla\times\boldsymbol{u}$ is the vorticity. The Stuart number (or interaction parameter), N, and Hartmann number, Ha, are related through $Ha^2 = ReN$. Equations (2.7)–(2.9) are referred to as simplified magnetohydrodynamic (SMHD) equations in this paper. We use u, v and w to denote the velocity components in the streamwise (x), wall-normal (y), and spanwise (z) directions, respectively.

3. Numerical methods

It is known to be very difficult to solve accurately the full MHD (FMHD) equations (2.1)–(2.5), because $\boldsymbol{u}$ and $\boldsymbol{B}$ are coupled nonlinearly and they have different timescales. Note that in most engineering applications, $Re \gg 1$ while $Re_m < 1$. Therefore, the diffusion timescales of the two variables are significantly different from each other, which inevitably requires a very small computational timestep so as to obtain accurate solutions. In a previous study (Choi *et al.* 1997), it was indeed shown from a coarse direct numerical simulation of MHD turbulent channel flow that a very small computational timestep (CFL $\ll 1$) is required for the FMHD equations. Also, in a two-dimensional simulation of vortex dipole interacting with a wall, the SMHD equations with a timestep corresponding to CFL ≈ 1 provided the same result as that from the FMHD equations with a very small timestep (Lim, Choi & Kim 1998). Therefore, in this paper, we use the SMHD equations.

The numerical method used to solve the SMHD equations (2.7)–(2.9) is based on a semi-implicit, fractional step method: the diffusion term in (2.7) is advanced in time with the Crank–Nicolson method, while the nonlinear and Lorentz force terms are advanced with a third-order Runge–Kutta (RK3) method:

$$\begin{aligned}\frac{\hat{u}_i^k - u_i^{k-1}}{\Delta t} &+ \gamma_k\frac{\partial u_i^{k-1}u_j^{k-1}}{\partial x_j} + \zeta_k\frac{\partial u_i^{k-2}u_j^{k-2}}{\partial x_j}\\ &= -2\alpha_k\frac{\partial p^{k-1}}{\partial x_i} + \frac{\alpha_k}{Re}\frac{\partial^2\hat{u}_i^k}{\partial x_j\partial x_j} + \frac{\alpha_k}{Re}\frac{\partial^2 u_i^{k-1}}{\partial x_j\partial x_j} + \gamma_k f_i^{k-1} + \zeta_k f_i^{k-2},\end{aligned} \tag{3.1}$$

$$\frac{\partial^2\psi^k}{\partial x_i\partial x_i} = \frac{1}{2\alpha_k\Delta t}\frac{\partial\hat{u}_i^k}{\partial x_i}, \tag{3.2}$$

$$u_i^k = \hat{u}_i^k - 2\alpha_k\Delta t\frac{\partial\psi^k}{\partial x_i}, \tag{3.3}$$

$$p^k = p^{k-1} + \psi^k - \frac{\alpha_k \Delta t}{Re} \frac{\partial^2 \psi^k}{\partial x_j \partial x_j}, \tag{3.4}$$

$$\frac{\partial^2 \phi^k}{\partial x_i \partial x_i} = \frac{\partial}{\partial x_i}(\epsilon_{ijl}\, u_j^k\, B_{ol}), \tag{3.5}$$

where $\boldsymbol{f} = N\{(-\nabla\phi + \boldsymbol{u} \times \boldsymbol{B}_o) \times \boldsymbol{B}_o\}$, $\hat{u}_i$ is the intermediate velocity, ψ is the pseudo-pressure, and ϵ_{ijk} is the permutation tensor. Also, Δt and k are the computational timestep and substep index, respectively, and α_k, γ_k and ζ_k are the coefficients of RK3 ($\alpha_1 = \frac{4}{15}$, $\gamma_1 = \frac{8}{15}$, $\zeta_1 = 0$; $\alpha_2 = \frac{1}{15}$, $\gamma_2 = \frac{5}{12}$, $\zeta_2 = -\frac{17}{60}$; $\alpha_3 = \frac{1}{6}$, $\gamma_3 = \frac{3}{4}$, $\zeta_3 = -\frac{5}{12}$).

All spatial derivatives are discretized with the second-order central-difference scheme. The suitability of using the second-order central difference scheme for direct numerical simulation of turbulent flows was discussed in Choi, Moin & Kim (1992) (see also Kong, Choi & Lee 2000). The Poisson equations for the pseudo-pressure and electric potential are solved using a transform method with the modified wavenumbers associated with the second-order central difference scheme, together with tridiagonal matrix inversion (see, for more details, Kim & Moin 1985). Numerical simulations are performed using $64 \times 97 \times 96$ grids in a computational domain of $3\pi(L_x) \times 2(L_y) \times \pi(L_z)$, respectively. The Reynolds number based on the laminar centreline velocity U_l and channel half-width δ is $Re = \rho U_l \delta/\mu = 3000$ (the bulk Reynolds number is $Re_b = \frac{4}{3}\rho U_l \delta/\mu = 4000$). The present simulation is carried out maintaining a constant mass flow rate in a channel, i.e. $\int_y \int_z \rho u \,\mathrm{d}z\,\mathrm{d}y = \frac{4}{3}\rho U_l \delta L_z =$ constant in time. The Reynolds number based on the turbulent centreline velocity U_c and channel half-width in the case of no magnetic field is $Re_c \approx 2330$, which corresponds to $Re_{\tau o} = \rho u_{\tau o}\delta/\mu \approx 140$, where $u_{\tau o}$ is the wall-shear velocity without magnetic field. The turbulent centreline velocity U_c and wall-shear velocity u_τ vary with the applied magnetic field. Therefore, unless otherwise specified, the laminar centreline velocity U_l is used for the characteristic velocity scale in the present study. The grid spacings in wall units based on $u_{\tau o}$ are $\Delta x^+ \approx 20.3$, $\Delta y^+_{min} \approx 0.3$, $\Delta y^+_{max} \approx 6.6$ and $\Delta z^+ \approx 4.5$. The spatial resolutions used in this study are very similar to those in Kim, Moin & Moser (1987); the present r.m.s. velocity fluctuation profiles without magnetic field ($Re_\tau \approx 140$) are in good agreement with the DNS data obtained from spectral simulations by Kim *et al.* (1987), ($Re_\tau = 180$) and Sureshkumar, Beris & Handler (1997), ($Re_\tau = 125$) when the Reynolds-number difference is taken into account. The CFL number is fixed as 1 which corresponds to $\Delta t \approx 0.06\delta/U_l$ ($\Delta t^+ = \Delta t u^2_{\tau o}/\nu \simeq 0.37$); the computational timestep less than $\Delta t^+ \simeq 0.4$ provided an accurate prediction of turbulence statistics in wall-bounded flow (Choi & Moin 1994). The boundary conditions at the non-conducting wall are

$$\boldsymbol{u}_{wall} = 0, \quad j_y|_{wall} = -\left.\frac{\partial \phi}{\partial y}\right|_{wall} = 0, \tag{3.6}$$

where j_y is the wall-normal component of the current density. The periodic boundary conditions are used in the streamwise and spanwise directions.

When there is no external electrical circuit, total current in the flow domain must be zero, i.e.

$$\int_0^{\pi} \int_{-1}^{1} \int_0^{3\pi} \boldsymbol{j}\,\mathrm{d}x\,\mathrm{d}y\,\mathrm{d}z = 0, \tag{3.7}$$

which can be easily confirmed by integrating (2.3). Thus, the volume integration of

(2.6) should be also zero, from which we have

$$\int j_x \,\mathrm{d}V = \int_0^{\pi}\int_{-1}^{1}\int_0^{3\pi}\left(-\frac{\partial\phi}{\partial x} + vB_{oz} - wB_{oy}\right)\mathrm{d}x\,\mathrm{d}y\,\mathrm{d}z = 0, \tag{3.8}$$

$$\int j_y \,\mathrm{d}V = \int_0^{\pi}\int_{-1}^{1}\int_0^{3\pi}\left(-\frac{\partial\phi}{\partial y} - uB_{oz} + wB_{ox}\right)\mathrm{d}x\,\mathrm{d}y\,\mathrm{d}z = 0, \tag{3.9}$$

$$\int j_z \,\mathrm{d}V = \int_0^{\pi}\int_{-1}^{1}\int_0^{3\pi}\left(-\frac{\partial\phi}{\partial z} + uB_{oy} - vB_{ox}\right)\mathrm{d}x\,\mathrm{d}y\,\mathrm{d}z = 0, \tag{3.10}$$

where B_o is the applied magnetic field which is a unit scalar. Equation (3.8) can be easily proved using $\int v\,\mathrm{d}V = \int w\,\mathrm{d}V = 0$ and the periodicity of ϕ in x. Likewise, (3.9) is also proved using (2.8) and $\int w\,\mathrm{d}V = 0$. In the case of a wall-normal magnetic field, there exists a mean spanwise electric field $\bar{E}_z$ which is independent of y (otherwise $\nabla \times \boldsymbol{E} = -\partial\boldsymbol{B}/\partial t \neq 0$) and is determined by (3.10) as

$$\bar{E}_z = -\frac{\mathrm{d}\bar{\phi}}{\mathrm{d}z} = -\tfrac{1}{2}B_{oy}\int_{-1}^{1}\langle u\rangle\,\mathrm{d}y, \tag{3.11}$$

where $\langle\,\rangle$ denotes the average over an (x, z)-plane. Note that $\bar{E}_z = 0$ for the streamwise and spanwise magnetic fields (Branover 1978). Hence, in all cases of streamwise, wall-normal and spanwise magnetic fields, the volume integration of the Lorentz force is zero.

In order to verify the appropriateness of using the SMHD equations for turbulent flow, we carried out simulations using both the SMHD and FMHD equations at the same Reynolds and Stuart numbers ($Re_{\tau o} \approx 140$, $N = 0.025$) in the case of uniform wall-normal magnetic field. We found that there is little difference between the SMHD and FMHD solutions at a low magnetic Reynolds number ($Re_m = 0.001$), even though the computational timestep, $\Delta t = 0.05\delta/U_l$, used for the SMHD equations is 100 times larger than that ($\Delta t = 0.0005\delta/U_l$) used for the FMHD equations. The FMHD solution with $\Delta t = 0.005\delta/U_l$ was completely different from that of the FMHD solution with $\Delta t = 0.0005\delta/U_l$ (see Lee & Choi 2000).

4. Turbulence statistics

In this study, three different Lorentz forces that result from applying uniform magnetic fields in the streamwise, wall-normal and spanwise directions to a conducting fluid in a channel are investigated. It is apparent from (2.7) that the most important parameter in the SMHD equations is the Stuart number, $N = \sigma B^{*2}\delta/\rho U_l$. Therefore, we fix the Reynolds number and change the Stuart number to investigate flow changes with respect to the strength of the applied magnetic field. Different ranges of the Stuart number are used for the streamwise, wall-normal and spanwise magnetic fields because the Stuart number for flow relaminarization or suppressing turbulent fluctuations is very different depending on the direction of the magnetic field: $N_x = 0 \sim 0.6$ for the streamwise magnetic field, $N_y = 0 \sim 0.1$ for the wall-normal magnetic field and $N_z = 0 \sim 0.1$ for the spanwise magnetic field. The corresponding Hartmann numbers, $Ha = (Re\,N)^{1/2} = \sqrt{\sigma/\mu}\,B^*\delta$, are $Ha_x \simeq 0 \sim 42$, $Ha_y \simeq 0 \sim 17$ and $Ha_z \simeq 0 \sim 17$, respectively. Flow variables are averaged in x, z and t, and a prime indicates perturbation from the average. The total averaging time to obtain the statistical quantities is about $300\delta/U_l$ ($\simeq 1920\nu/u_{\tau o}^2$).

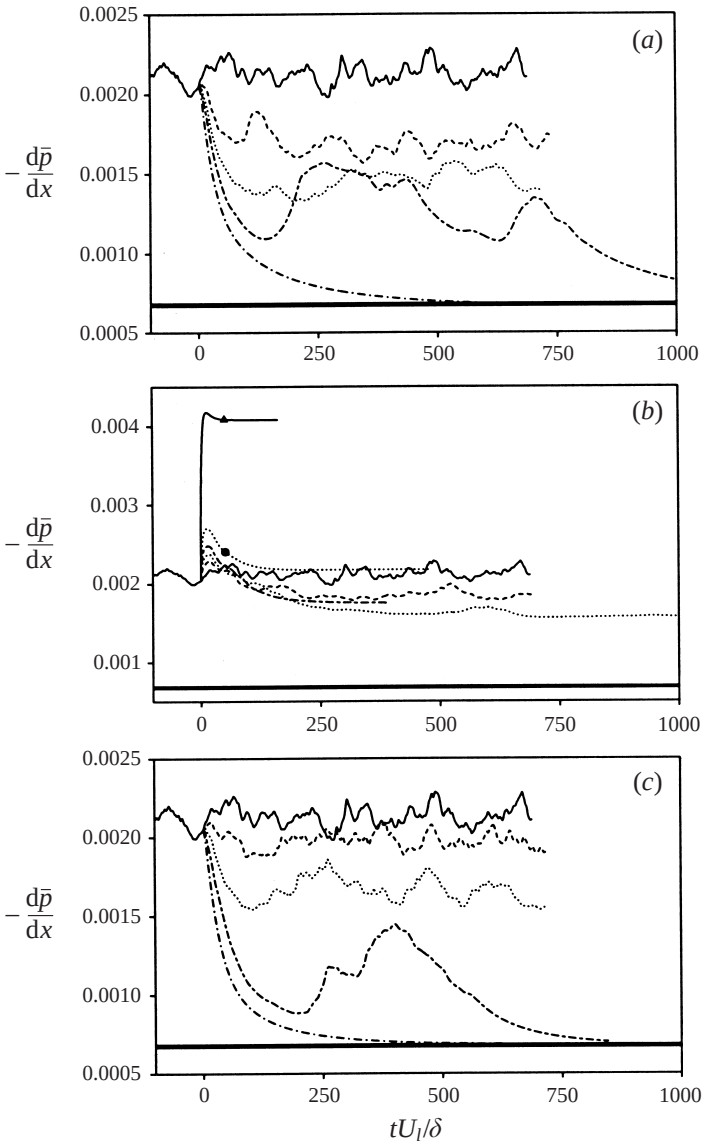

FIGURE 1. Time histories of the mean pressure gradient: (*a*) - - - - -, $N_x = 0.1$; · · · · · ·, $N_x = 0.2$; — - —, $N_x = 0.3$; — · —, $N_x = 0.6$; (*b*) - - - - -, $N_y = 0.006$; · · · · · ·, $N_y = 0.01$; — - —, $N_y = 0.015$; · · · · · · with ●, $N_y = 0.025$; —— with ▲, $N_y = 0.1$; (*c*) - - - - -, $N_z = 0.01$; · · · · · ·, $N_z = 0.025$; — - —, $N_z = 0.05$; — · —, $N_z = 0.1$. The solid line denotes the mean pressure gradient without magnetic field. $-d\bar{p}/dx = 0.00067$ (thick solid line) corresponds to the value for laminar flow.

4.1. *Drag*

Figure 1 shows the time histories of the mean pressure gradient required to drive a fixed mass flow rate in a channel for the cases with and without magnetic field. For the wall-normal magnetic field (figure 1*b*), the change in the skin friction is explained in terms of suppression of turbulence and the Hartmann effect. The former is associated with the direct action of the magnetic field on turbulence and thus decreases the skin friction, whereas the latter is associated with the change in the mean velocity profile

via formation of thin layers ($\sim Ha^{-1}$) at non-conducting walls (Tsinober 1990*a*), resulting in the increase of the skin friction. As shown in figure 1(*b*), the skin friction decreases at low Stuart numbers ($N_y < 0.025$) because the drag reduction due to turbulence suppression is bigger than the drag increase due to the Hartmann effect. When $N_y \geqslant 0.025$, drag increases owing to the dominance of the Hartmann effect. The greatest drag reduction is obtained at $N_y = 0.01\,(Ha/Re_c \times 10^4 \approx 23)$, yielding about 27% drag reduction. The present result is very similar to the data presented in Reed & Lykoudis (1978) (see also Gardner & Lykoudis 1971): the minimum drag existed at $Ha/Re_c \times 10^4 \simeq 23$ in the skin friction coefficient *vs.* Ha/Re_c.

On the other hand, a magnetic field in the streamwise or spanwise direction does not directly interact with the mean flow but with turbulent fluctuations. It is shown in figures 1(*a*) and 1(*c*) that substantial skin-friction reductions are obtained by applying the magnetic fields in the streamwise and spanwise directions. The flow becomes laminar at $N_z \geqslant 0.05$, while the flow is laminar at $N_x \geqslant 0.3$, indicating that the spanwise magnetic field is much more effective in reducing drag than the streamwise magnetic field. Harris (1960) suggested that, under a longitudinal (streamwise) magnetic field, the drag should be reduced considerably and the velocity profile should be parabolic, which was confirmed experimentally by Fraim & Heiser (1968). Tsinober (1990*a*) performed experiments by varying the aspect ratio (height to width) of ducts, where a magnetic field was applied in the direction of the width. The case of the smallest aspect ratio with a magnetic field in a duct is similar to the present case of the spanwise magnetic field in a channel. Tsinober's data showed that the smallest aspect ratio resulted in the largest drag reduction. The present result appears to be in qualitative agreement with Tsinober's experimental results. Orlandi (1996) presented a preliminary result of MHD turbulent pipe flow using the direct numerical simulation technique for the FMHD equations. It was also shown that the azimuthal (spanwise) magnetic field was more efficient in reducing drag than the axial (streamwise) magnetic field.

The mean velocity profiles normalized by the actual wall-shear velocities u_τ were plotted in wall coordinates for the cases with and without magnetic field (see Lee & Choi 2000). Upward shifts in the log-law for the cases of the streamwise and spanwise magnetic fields were clearly observed, which had previously been observed in most of drag-reducing flows such as riblets (Choi, Moin & Kim 1993), polymers (Walker & Tiederman 1990) and active blowing/suction (Choi, Moin & Kim 1994). For the wall-normal magnetic field, upward shifts in the log-law were observed at $N_y < 0.025$ as in the cases of streamwise and spanwise magnetic fields, while a significant downward shift was observed at $N_y = 0.1$ owing to the Hartmann effect. A similar observation was also made in the experimental work of Reed & Lykoudis (1978) and in the numerical (LES) work of Shimomura (1991).

4.2. *Turbulence intensities, Reynolds shear stress and vorticity fluctuations*

Turbulence intensities in the channels with applied magnetic fields are shown in figure 2, respectively, together with those in the channel without magnetic field. In the case of streamwise magnetic field, as the Stuart number increases, the streamwise velocity fluctuations increase but the wall-normal and spanwise velocity fluctuations decrease. This increase of the streamwise velocity fluctuations was also reported in Orlandi (1996) and polymer drag reduction by Walker & Tiederman (1990), but the reason was not clearly explained in a convincing manner. At a strong streamwise magnetic field, we will discuss the changes in the turbulence intensities, especially in the streamwise velocity fluctuations, in detail in § 5. In the cases of wall-normal and

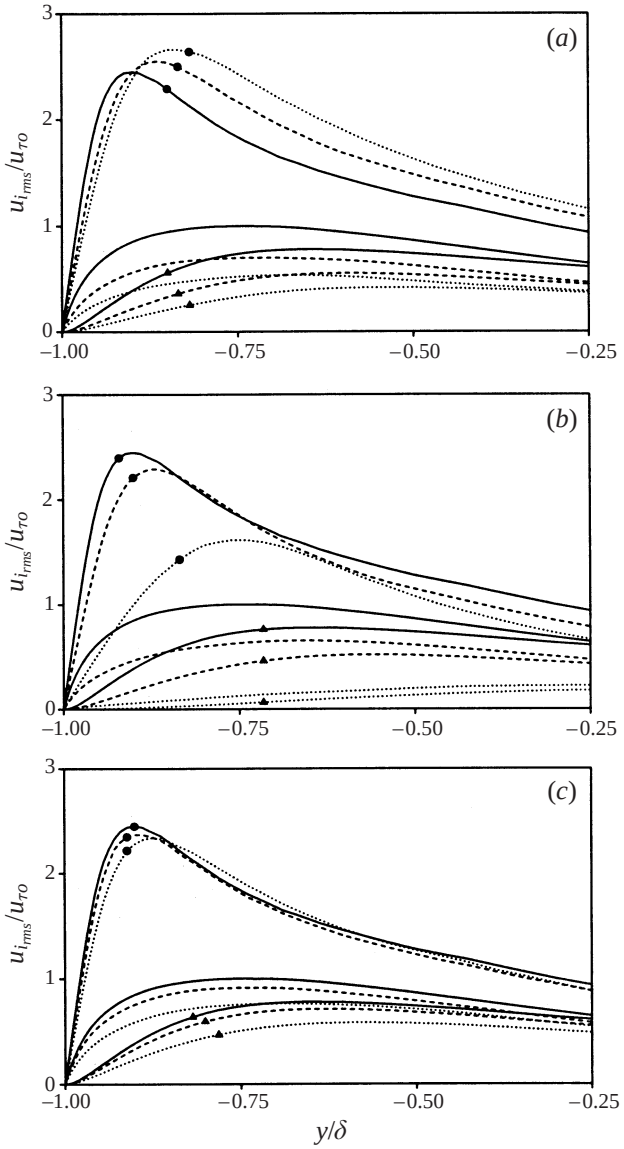

FIGURE 2. Root-mean-square velocity fluctuations normalized by the wall-shear velocity: (*a*) - - - - -, $N_x = 0.1$; · · · · · ·, $N_x = 0.2$; (*b*) - - - - -, $N_y = 0.006$; · · · · · ·, $N_y = 0.01$; (*c*) - - - - -, $N_z = 0.01$; · · · · · ·, $N_z = 0.025$. Lines with ●, u_{rms}; lines with ▲, v_{rms}; lines, w_{rms}. Note that $u_{\tau o}$ is the wall-shear velocity without magnetic field. The solid line denotes the velocity fluctuations without magnetic field.

spanwise magnetic fields, all three components of turbulence intensities decrease as the Stuart number increases, indicating that the detailed mechanism responsible for turbulence modification from the streamwise magnetic field is different from those from the wall-normal and spanwise magnetic fields. Reed & Lykoudis (1978) showed a similar suppression of the turbulence intensities for the wall-normal magnetic field. It is very clear from figure 2 that the wall-normal magnetic field is most effective in reducing the turbulent fluctuations (see also § 5).

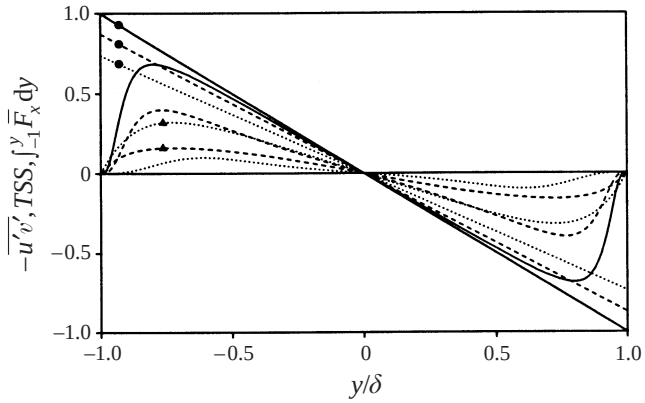

FIGURE 3. Reynolds shear stress ($-\overline{u'v'}$; lines), total shear stress ($-\overline{u'v'} + (1/Re_{\tau o})\partial\bar{u}/\partial y + \int_{-1}^{y} \bar{F}_x \, dy \equiv TSS$; lines with ●) and integral of mean streamwise Lorentz force ($\int_{-1}^{y} \bar{F}_x \, dy$; lines with ▲) normalized by the wall-shear velocity in the case of wall-normal magnetic field: - - - - -, $N_y = 0.006$; ·····, $N_y = 0.01$. The solid line denotes the Reynolds shear stress without magnetic field.

The turbulent kinetic energy showed the same trend as the streamwise velocity fluctuations (not shown here), because u_{rms} is much larger than v_{rms} and w_{rms}. The pressure fluctuations were also substantially reduced throughout the channel with magnetic fields (not shown here).

The Reynolds shear stress for the case of a wall-normal magnetic field is shown in figure 3. Also shown in figure 3 is the total shear stress, $-\overline{u'v'} + (1/Re_{\tau o})\partial\bar{u}/\partial y + \int_{-1}^{y} \bar{F}_x \, dy$, where $\bar{F}_x$ is the mean Lorentz force in the streamwise direction. For the streamwise and spanwise magnetic fields, $\bar{F}_x$ is zero. In the case of a wall-normal magnetic field, the integral of $\bar{F}_x$ due to the mean spanwise electric field (3.11) is not negligible. The mean Lorentz force is maximum at the wall, rapidly decreases away from the wall, and becomes negative in the channel-centre region (Lee & Choi 2000), which clearly indicates the Hartmann effect. Taking the average of the streamwise momentum equation non-dimensionalized with $u_{\tau o}^2/\delta$ over time and space (x and z) provides

$$\frac{\partial}{\partial y}\left(-\overline{u'v'} + \frac{1}{Re_{\tau o}}\frac{\partial \bar{u}}{\partial y}\right) + \bar{F}_x = \frac{d\bar{p}}{dx} = \text{constant}. \tag{4.1}$$

In the fully developed channel flow considered here, the total shear stress is a straight line when the flow reaches an equilibrium state. The computed results clearly indicate that this is the case (figure 3). The slope of the total shear stress is reduced as the Stuart number increases. A significant reduction in the Reynolds shear stress throughout the channel is also observed in figure 3. Reed & Lykoudis (1978) measured the Reynolds shear stress with a wall-normal magnetic field and found that $-\overline{u'v'}$ essentially vanishes while the turbulent energy is still high enough. The same conclusion can be made in this study by comparing the reduced amount of u_{rms} (or turbulent kinetic energy) with that of $-\overline{u'v'}$ (figures 2*b* and 3). A similar observation was made in the cases of streamwise and spanwise magnetic fields; that is, the Reynolds shear stress and total shear stress decrease as the Stuart number increases (see Lee & Choi 2000 for more detail).

Root-mean-square streamwise-vorticity fluctuations are significantly reduced owing

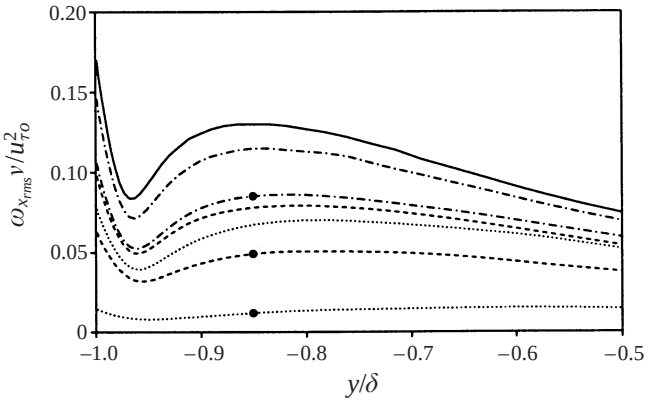

FIGURE 4. Root-mean-square streamwise vorticity fluctuations normalized by the wall-shear velocity and the kinematic viscosity: -----, $N_x = 0.1$; ----- with ●, $N_x = 0.2$; ·····, $N_y = 0.006$; ····· with ●, $N_y = 0.01$; —·—, $N_z = 0.01$; —·— with ●, $N_z = 0.025$. The solid line denotes the streamwise vorticity fluctuations without magnetic field.

to the magnetic field (figure 4). Other components of the vorticity fluctuations are also substantially reduced owing to the magnetic field (Lee & Choi 2000). The y-locations of the local maxima of the streamwise vorticity fluctuations move further away from the wall as compared to that without magnetic field, suggesting that the sweep motion induced by the streamwise vortices in MHD channel flows is less effective in producing a high skin-friction region.

The effect of the magnetic field on the streamwise vorticity can be investigated from the vorticity equation:

$$\frac{\partial \omega_x}{\partial t} + (\boldsymbol{u}\cdot\nabla)\omega_x - (\boldsymbol{\omega}\cdot\nabla)u - \frac{1}{Re}\nabla^2\omega_x = \begin{cases} -N\dfrac{\partial^2\phi}{\partial x^2} & \text{for } N_x, \\ -N\left(\dfrac{\partial^2\phi}{\partial y\,\partial x} + \dfrac{\partial w}{\partial y}\right) & \text{for } N_y, \\ -N\left(\dfrac{\partial^2\phi}{\partial z\,\partial x} - \dfrac{\partial v}{\partial z}\right) & \text{for } N_z. \end{cases} \tag{4.2}$$

It can be seen that the Lorentz force has two terms: one is associated with the electric potential and the other is related to the velocity gradient. The velocity gradient terms, $\partial w/\partial y$ and $\partial v/\partial z$, are much larger than the electric potential terms, $\partial^2\phi/\partial x^2$, $\partial^2\phi/\partial y\,\partial x$ and $\partial^2\phi/\partial z\,\partial x$ (not shown here). Therefore, the reduction of $\omega_{x_{rms}}$ is smallest in the case of a streamwise magnetic field. Equation (4.2) shows that the Lorentz force induced from the wall-normal or spanwise magnetic field is negatively correlated with one or the other contributing velocity derivative of the streamwise vorticity ($\omega_x = \partial w/\partial y - \partial v/\partial z$). Hence, the reduction in the intensity of the streamwise vorticity is apparent for both cases. In a turbulent boundary layer, the r.m.s. value of $\partial w/\partial y$ is much larger than that of $\partial v/\partial z$ near the wall. Therefore, the wall-normal magnetic field is more effective than the spanwise magnetic field in weakening the near-wall streamwise vorticity in a turbulent boundary layer (note that ω_x becomes nearly zero even at $N_y = 0.01$), even though the wall-normal magnetic field interacts directly with the mean flow and increases drag at high N_y.

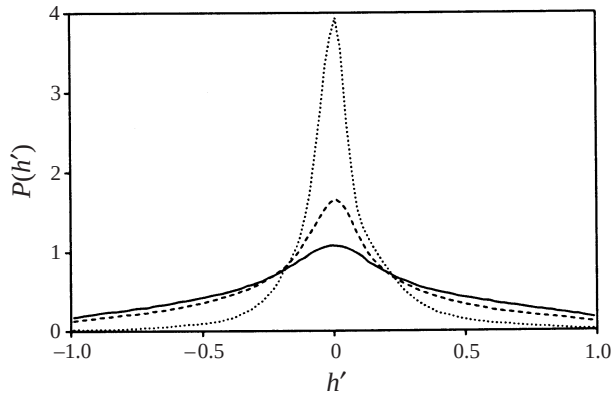

FIGURE 5. Probability density function of the relative helicity density fluctuations at $y^+ = yu_{\tau o}/\nu \approx 10$: - - - - -, $N_x = 0.1$; · · · · · ·, $N_x = 0.2$. The solid line denotes $P(h')$ without magnetic field.

4.3. *Helicity density*

The helicity density, $H = \boldsymbol{u}\cdot\boldsymbol{\omega}$, is known to play an important role in magnetohydrodynamics (Moffatt 1978) and is thought to be an important quantity in all kinds of turbulent flow (Tsinober 1990*b*). The relative helicity density fluctuation is a dimensionless quantity defined by $h' = \boldsymbol{u}'\cdot\boldsymbol{\omega}'/(|\boldsymbol{u}'|\,|\boldsymbol{\omega}'|) = \cos\theta$, where θ is the angle between the velocity and vorticity fluctuation vectors. When $h' = 0$, the vorticity fluctuation vector is perpendicular to the velocity fluctuation vector, whereas they are parallel to each other when $h' = \pm 1$. Figure 5 shows the probability density function (p.d.f.) of h' at $y^+ \approx 10$ in the case of a streamwise magnetic field. Without a magnetic field, the vorticity and velocity fluctuations are not aligned. This poor alignment is due to the fact that near the wall the vorticity fluctuation is dominated by the spanwise component but the velocity fluctuation is dominated by the streamwise component. The misalignment increases as the wall is approached. Outside the buffer layer where turbulence becomes more isotropic, the p.d.f. is relatively flat (not shown here). With the magnetic fields, the misalignment increases at all y-locations, resulting in very small helicity fluctuations and strong peaks of $P(h')$ at $h' = 0$ in the wall region. This decrease of helicity fluctuations means that the near-wall vortical structures in MHD channel flows become less helical. Similar behaviours are also observed for the cases of wall-normal and spanwise magnetic fields.

4.4. *Lorentz force*

For incompressible flow, the temporal change of $\overline{u'^2}$ non-dimensionalized with $u_{\tau o}^3/\delta$ is given as follows:

$$\frac{\partial}{\partial t}\overline{u'^2} = \underbrace{-2\overline{u'v'}\frac{\partial \bar{u}}{\partial y}}_{P_{11}} \underbrace{-\frac{\partial}{\partial y}\overline{u'^2v'}}_{T_{11}} \underbrace{+2\overline{p'\frac{\partial u'}{\partial x}}}_{\phi_{11}} \underbrace{+\frac{1}{Re_{\tau o}}\frac{\partial^2\overline{u'^2}}{\partial y^2}}_{D_{11}} \underbrace{-\frac{2}{Re_{\tau o}}\overline{\frac{\partial u'}{\partial x_j}\frac{\partial u'}{\partial x_j}}}_{\epsilon_{11}} \underbrace{+2\overline{u'F_x'}}_{F_{11}}, \tag{4.3}$$

where the last term in the equation represents the contribution from the Lorentz force. The temporal changes of $\overline{v'^2}$ and $\overline{w'^2}$ can be similarly given as (4.3). Each term of (4.3) will be examined to investigate the behaviour of the streamwise velocity fluctuations in the presence of a strong magnetic field (§ 5.2). It can be shown easily from (2.7) that the component of the Lorentz force in a direction parallel to the magnetic field

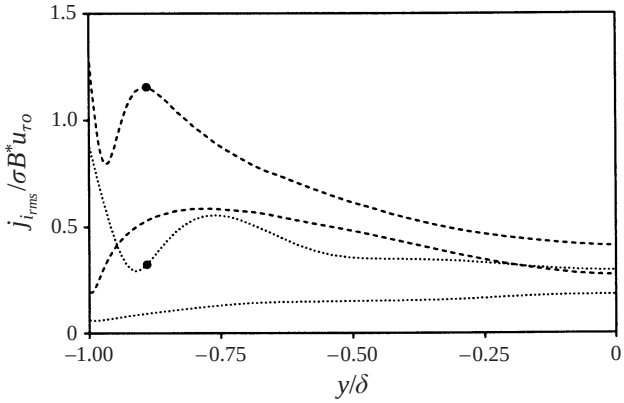

FIGURE 6. Root-mean-square current density fluctuations: - - - - -, $N_y = 0.006$; · · · · · ·, $N_y = 0.01$. Lines, $j_{x_{rms}}$; lines with ●, $j_{z_{rms}}$.

vector is exactly zero; for example, for $\boldsymbol{B}_o = (0, 1, 0)$,

$$F'_x = -Nj'_z = N\left(\frac{\partial \phi'}{\partial z} - u'\right), \quad F'_y = 0, \quad F'_z = Nj'_x = N\left(-\frac{\partial \phi'}{\partial x} - w'\right). \tag{4.4}$$

Therefore, the turbulence intensities in the directions orthogonal to the magnetic field vector are directly affected by the Lorentz force, whereas that in the direction parallel to the magnetic field vector is indirectly affected through the changes in other components of velocity fluctuations. The negative correlation between u'_α and F'_α decreases $\overline{u'_\alpha u'_\alpha}$ in time (see, for example, (4.3) and (4.4) for $\alpha = 1$).

All three components of root-mean-square current density fluctuations decrease as the Stuart number increases, irrespective of the direction of the applied magnetic field, because all the r.m.s. values of $-\nabla\phi$ and $\boldsymbol{u} \times \boldsymbol{B}_o$ are associated with the r.m.s. values of the corresponding velocity and vorticity fluctuations (see (2.6) and (2.8)) and thus decrease with increasing N (see, for example, figure 6 for N_y). On the other hand, the Lorentz force fluctuations show non-monotonic behaviour with respect to N. That is, at small N, $\boldsymbol{F}_{rms}$ increases with increasing N because increase of N is bigger than decrease of $\boldsymbol{j}'$, whereas it decreases with increasing N at relatively large N owing to a significant decrease of $\boldsymbol{j}'$ (see Lee & Choi 2000 for more detail). Note that there exist non-zero Lorentz force fluctuations at the wall, because $\partial\phi/\partial y\,|_{wall} = 0$, but $\partial\phi/\partial x\,|_{wall}$ and $\partial\phi/\partial z\,|_{wall}$ are not zero.

The work performed by the Lorentz force, $\overline{u'_j F'_j}$, is given by

$$\overline{\boldsymbol{u}' \cdot \boldsymbol{F}'} = -N\overline{\boldsymbol{j}' \cdot \boldsymbol{j}'} - N\nabla \cdot (\overline{\phi' \boldsymbol{j}'}), \tag{4.5}$$

where the first term in the right-hand side is the Joule dissipation (J_k) which is always negative and the second term is zero when it is volume integrated. Thus, the global work, $\int \overline{\boldsymbol{u}' \cdot \boldsymbol{F}'}\,\mathrm{d}V$, is the same as the global Joule dissipation, $-N\int \overline{\boldsymbol{j}' \cdot \boldsymbol{j}'}\,\mathrm{d}V$. For all the cases investigated in this study, $\overline{\boldsymbol{u}' \cdot \boldsymbol{F}'} \simeq -N\overline{\boldsymbol{j}' \cdot \boldsymbol{j}'}$ near the channel centre, but this is not true near the wall, indicating that the second term in the right-hand side of (4.5) is not negligible near the wall (see Lee & Choi 2000 for more detail). The production ($P_k = -\overline{u'_i u'_j}\,\partial\overline{u}_i/\partial x_j$) and viscous dissipation ($\epsilon_k = -(1/Re_{\tau o})(\overline{\partial u'_i/\partial x_j + \partial u'_j/\partial x_i)\partial u'_j/\partial x_i}$) of the turbulent kinetic energy ($k \equiv \frac{1}{2}u'_i u'_i$) are

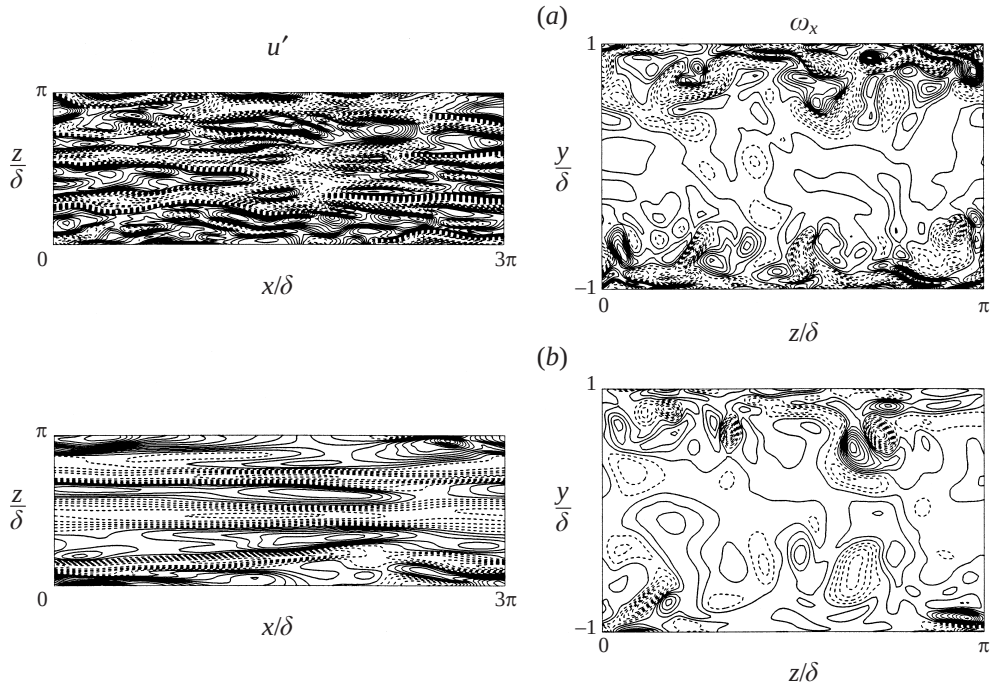

FIGURE 7. Contours of the instantaneous streamwise velocity fluctuations in an (x, z)-plane at $y^+ = yu_{\tau o}/\nu \approx 10$ and streamwise vorticity fluctuations in a (y, z)-plane: (*a*) no magnetic field; (*b*) $N_y = 0.006$. The contour levels of $u'/u_{\tau o}$ range from -4.5 to 6.5 by increments of 0.5, and those of $\omega_x \delta/u_{\tau o}$ range from -60 to 60 by increments of 5. Negative values are dashed.

significantly reduced by the applied magnetic field throughout the channel (see Lee & Choi 2000).

5. Turbulence structures

As mentioned in § 4, the turbulence statistics in the channel with magnetic fields are substantially different from those in the channel without a magnetic field. A relatively small amount of magnetic field changes the turbulence statistics throughout the channel. Differences in the turbulence statistics of MHD channel flows reveal that, despite comparable drag reductions, the structures are affected differently. In this section, we focus on turbulence structures in the channel with a weak or strong magnetic field by examining instantaneous flow fields.

5.1. *Weak to moderate magnetic field* (*small to intermediate Stuart number*)

Contours of the instantaneous streamwise velocity fluctuations at $y^+ \approx 10$ and the streamwise vorticity fluctuations in a crossflow plane in the channel with magnetic fields are compared to those in the channel without a magnetic field in figure 7. The streaky structures are substantially weakened and the streak spacing appears to be larger than that in the channel without a magnetic field. This observation was also confirmed with two-point correlations of the velocity fluctuations (not shown here). The reduction in the intensity of the streamwise vorticity is also apparent in this figure.

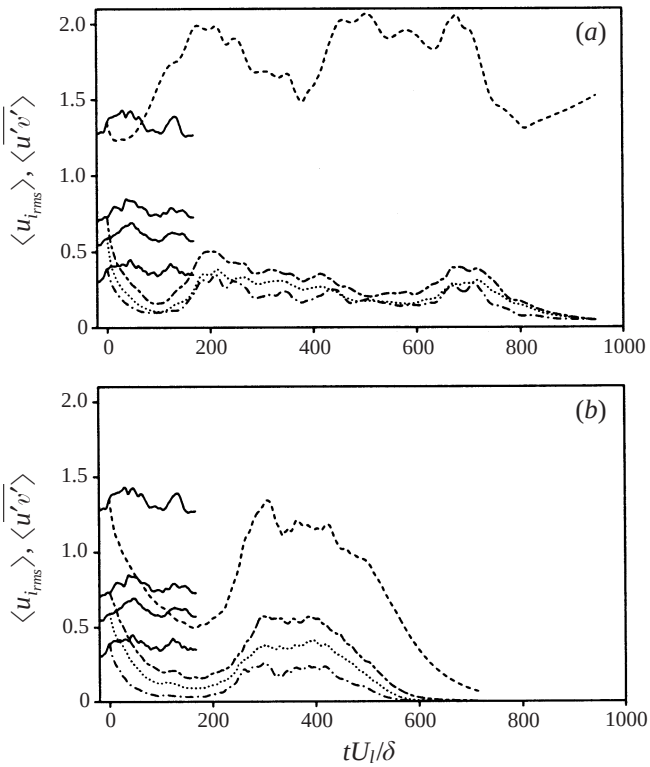

FIGURE 8. Time histories of the volume-averaged velocity fluctuations and Reynolds shear stress: (*a*) $N_x = 0.3$; (*b*) $N_z = 0.05$. The solid lines denote for the case without magnetic field. - - - - -, $\langle u_{rms} \rangle$; ·····, $\langle v_{rms} \rangle$; — - —, $\langle w_{rms} \rangle$; —·—, $\langle \overline{u'v'} \rangle$. Here, $\langle u_{i_{rms}} \rangle = (1/V) \int u_{i_{rms}}/u_{\tau o} \, \mathrm{d}V$ and $\langle \overline{u'v'} \rangle = (1/V) \int |\overline{u'v'}|/u_{\tau o}^2 \, \mathrm{d}V$.

Zikanov & Thess (1998) showed from their forced MHD turbulence that, at intermediate magnetic field strength, the flow exhibits an intermittent behaviour, characterized by organized quasi-two-dimensional evolution lasting several eddy-turnover times, which is interrupted by strong three-dimensional turbulent bursts. In this study, similar turbulent bursts were observed during relaminarization at intermediate Stuart numbers: in figure 1, the drag histories at $N_x = 0.3$ and $N_z = 0.05$ show some turbulent bursts. Volume-averaged values of the turbulence intensities and Reynolds shear stress also show very similar temporal behaviours to that of drag (figure 8). However, turbulent bursts occur only once or twice during the relaminarization, which is very different from the case of forced MHD turbulence. The Reynolds number investigated in this study is a subcritical Reynolds number and thus disturbances with finite amplitudes are required to drive the flow to a turbulent flow during the relaminarization. Therefore, a similar behaviour of quasi-periodic turbulent bursts observed in a forced MHD turbulence may be observed in a turbulent channel flow at supercritical Reynolds numbers.

5.2. *Strong magnetic field* (*large Stuart number*)

Figure 9 shows the time histories of the volume-averaged turbulence intensities, Reynolds shear stress and vorticity fluctuations, where the integral is taken over the computational domain. In the channel with a strong streamwise magnetic field,

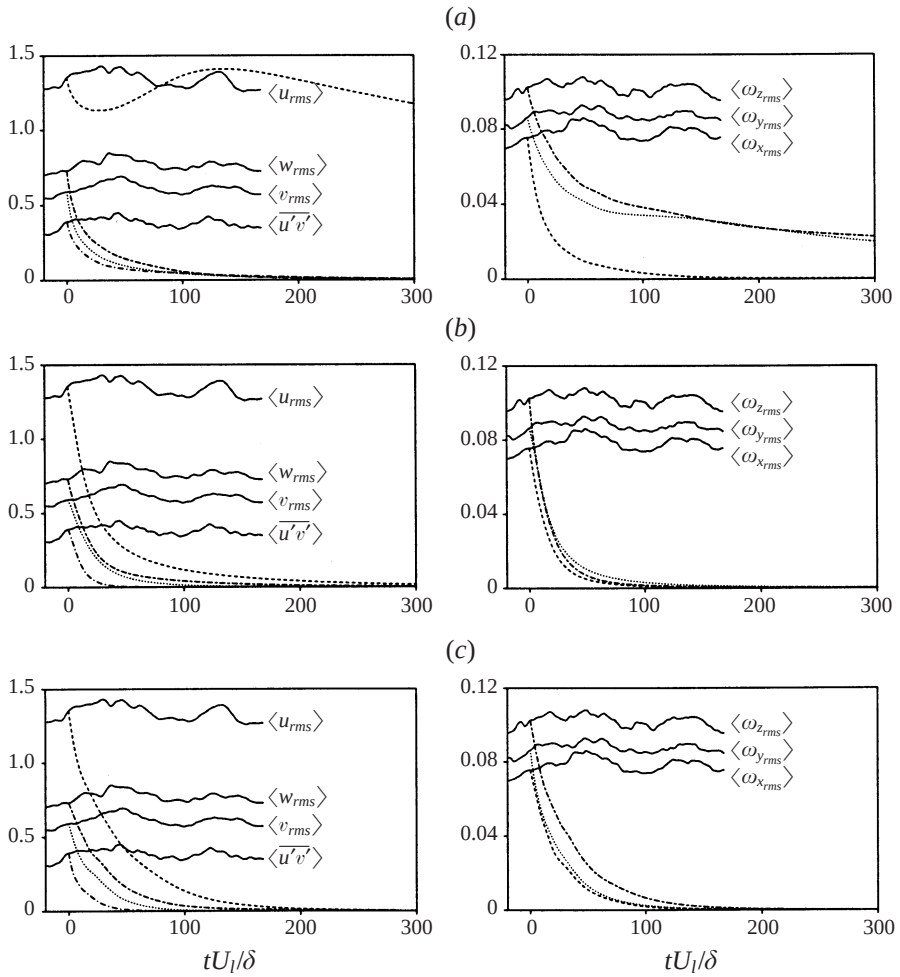

FIGURE 9. Time histories of the volume-averaged velocity fluctuations, Reynolds shear stress and vorticity fluctuations: (*a*) $N_x = 0.6$; (*b*) $N_y = 0.1$; (*c*) $N_z = 0.1$. The solid lines denote for the case without magnetic field. Here, $\langle u_{i_{rms}} \rangle = (1/V) \int u_{i_{rms}}/u_{\tau o}\, \mathrm{d}V$, $\langle \overline{u'v'} \rangle = (1/V) \int |\overline{u'v'}|/u_{\tau o}^2\, \mathrm{d}V$ and $\langle \omega_{i_{rms}} \rangle = (1/V) \int \omega_{i_{rms}}\, \nu/u_{\tau o}^2\, \mathrm{d}V$.

the streamwise velocity fluctuations still exist and slowly decay, even though other components of the velocity fluctuations and Reynolds shear stress vanish (figure 9*a*). This phenomenon is in good agreement with the experimental results in Tsinober (1990*a*), who showed that the velocity fluctuations parallel to the magnetic field are far from being zero. The wall-normal and spanwise vorticity fluctuations ($\omega_{y\,rms}$ and $\omega_{z\,rms}$) still exist owing to the two-dimensional characteristics of the streamwise velocity fluctuations $u(y, z)$, which will be confirmed later by the anisotropy invariant map for the vorticity (figure 14*a*). In the cases of strong wall-normal and spanwise magnetic fields, all the turbulence intensities, Reynolds shear stress and vorticity fluctuations decrease rapidly and become zero (figure 9*b*, *c*), which is in good agreement with the experiment in an annular infinitely long channel with a wall-normal magnetic field (Tsinober 1990*a*).

The changes in the streamwise velocity fluctuations may be understood from the volume integration of (4.3). Here, $\int T_{11}\,\mathrm{d}V = 0$ owing to the no-slip condition. $\int D_{11}\,\mathrm{d}V$ is two orders of magnitude smaller than those of other terms, $\int P_{11}\,\mathrm{d}V$, $\int \phi_{11}\,\mathrm{d}V$, $\int \epsilon_{11}\,\mathrm{d}V$ and $\int F_{11}\,\mathrm{d}V$ (note that $\overline{u'F_x'} = 0$ for the streamwise magnetic field and $\int F_{11}\,\mathrm{d}V$ is of similar magnitude to other terms for the wall-normal and spanwise magnetic fields). Time histories of these terms are shown in figure 10. For the strong streamwise magnetic field (figure 10*a*), an abrupt change of $\langle\phi_{11}\rangle$ at the beginning of applying the magnetic field is due to the abrupt increase of the pressure fluctuations. At $tU_l/\delta \leqslant 23$, $\langle u_{rms}\rangle$ decreases (figure 9*a*), because the sum of the absolute magnitudes of $\langle\phi_{11}\rangle$ and $\langle\epsilon_{11}\rangle$ which make a negative contribution to $\partial\overline{u'^2}/\partial t$ is a little bigger than that of $\langle P_{11}\rangle$. At $23 < tU_l/\delta \leqslant 135$, $\langle u_{rms}\rangle$ increases because the absolute magnitude of $\langle P_{11}\rangle$ is greater than that of $\langle\epsilon_{11}\rangle$. Note that $\langle\phi_{11}\rangle$ quickly decays in time. At $tU_l/\delta > 135$, $\langle u_{rms}\rangle$ decreases slowly owing to $\langle\epsilon_{11}\rangle$. In the cases of strong wall-normal and spanwise magnetic fields, $\langle u_{rms}\rangle$ decreases owing to an additional term of $\langle F_{11}\rangle$ which makes a negative contribution to $\partial\overline{u'^2}/\partial t$ (figure 10*b*, *c*).

The time histories of the volume-averaged production and viscous dissipation of the turbulent kinetic energy, and Joule dissipation are shown in figure 11. All values are substantially reduced by the applied magnetic field throughout the channel. Davidson (1995, 1997) showed that flow structures are elongated in the direction of the magnetic field in magnetic damping of jets and vortices because the Joule dissipation should be minimized to conserve the momentum. This argument can be easily understood from taking the curl of (2.6):

$$\nabla \times \boldsymbol{j} = (\boldsymbol{B}_o \cdot \nabla)\boldsymbol{u}, \tag{5.1}$$

from which it can be shown that the current density is potential ($\boldsymbol{j} = -\nabla\varphi$) when the velocity is uniform in the direction of the applied magnetic field. With $\nabla^2\varphi = 0$ (from $\nabla \cdot \boldsymbol{j} = 0$) and $\partial\varphi/\partial y|_{wall} = 0$, $\varphi \equiv$ constant. Thus, the Joule dissipation disappears in this case. Accordingly, the Joule dissipation can be reduced by aligning the velocity field with the direction of the magnetic field. For the strong streamwise magnetic field, the decrease of the Joule dissipation is much more rapid than that of the viscous dissipation of the turbulent kinetic energy (figure 11*a*), because the streamwise velocity fluctuations are close to two-dimensional in the sense that they become independent of the direction of the magnetic field, that is, $u = u(y, z)$. After the Joule dissipation disappears, the streamwise velocity fluctuations are dissipated only by the viscosity. Hence, the streamwise velocity fluctuations exist for a long time, but they eventually vanish because the absolute magnitude of the viscous dissipation is greater than that of the production. On the other hand, in the cases of strong wall-normal and spanwise magnetic fields, the Joule dissipation is about the same magnitude as the viscous dissipation, and the decrease of the production is most rapid (figure 11*b*, *c*).

It is well known that turbulence structures are markedly elongated in the direction of the magnetic field, when it is strong enough (Sommeria & Moreau 1982). Also, in the case of a strong magnetic field (large interaction parameter) a rapid transformation to a purely two-dimensional steady state is obtained for forced MHD turbulence (Zikanov & Thess 1998). The elongation of turbulence structures in a channel along the direction of the applied magnetic field is shown clearly in figure 12, where the iso-surfaces of each vorticity component are plotted. We have also drawn the iso-surfaces of λ_2 (second largest and negative eigenvalue of $S_{ik}S_{kj} + \Omega_{ik}\Omega_{kj}$, where S_{ij} and Ω_{ij} are the symmetric and antisymmetric parts of the velocity gradient tensor) suggested by

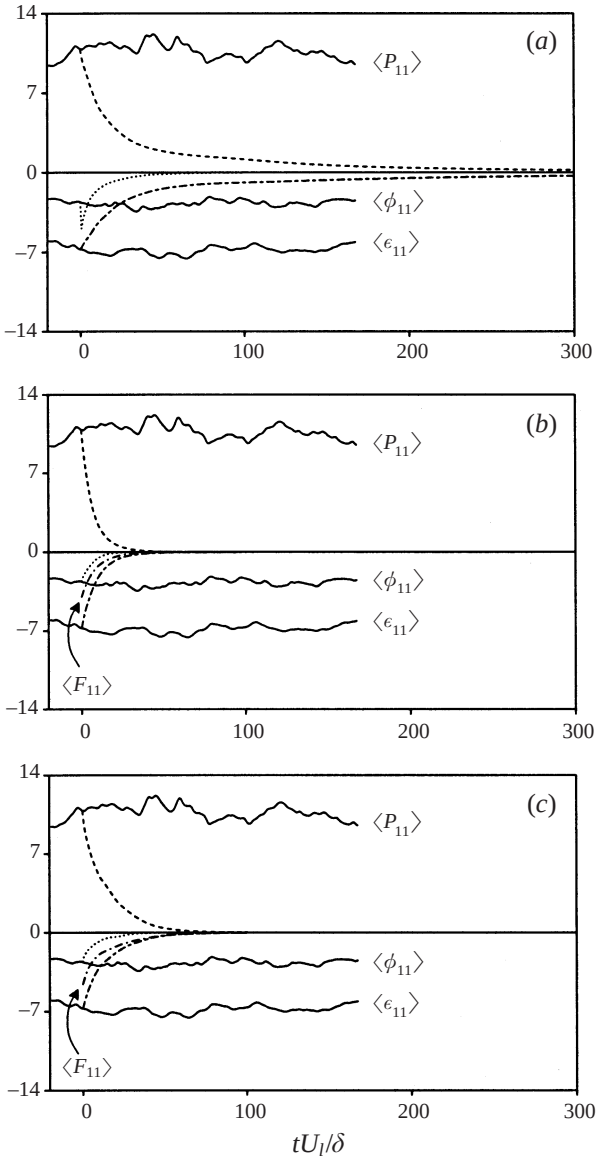

FIGURE 10. Time histories of the volume-averaged production $\langle P_{11}\rangle$, pressure–strain correlation $\langle \phi_{11}\rangle$, dissipation $\langle \epsilon_{11}\rangle$ and work performed by the Lorentz force fluctuations $\langle F_{11}\rangle$ normalized by $u_{\tau o}^3/\delta$: (*a*) $N_x = 0.6$; (*b*) $N_y = 0.1$; (*c*) $N_z = 0.1$. The solid lines denote for the case without magnetic field. Here, $\langle \bullet \rangle = (1/V)\int \bullet \, \mathrm{d}V$.

Jeong & Hussain (1995) as a vortex-identification method and found that they look similar to those of the streamwise vorticity fluctuations. In the channel without a magnetic field, the near-wall vortical structures are clearly observed (figure 12*a*). With magnetic fields, the strengths of the vorticities are significantly reduced (figures 12*b–d*). It can be seen from figures 12(*b*) and 12(*d*) that all three components of the vorticity fluctuations are elongated in the direction of the applied magnetic field when a strong streamwise or spanwise magnetic field is applied. For a strong wall-normal magnetic

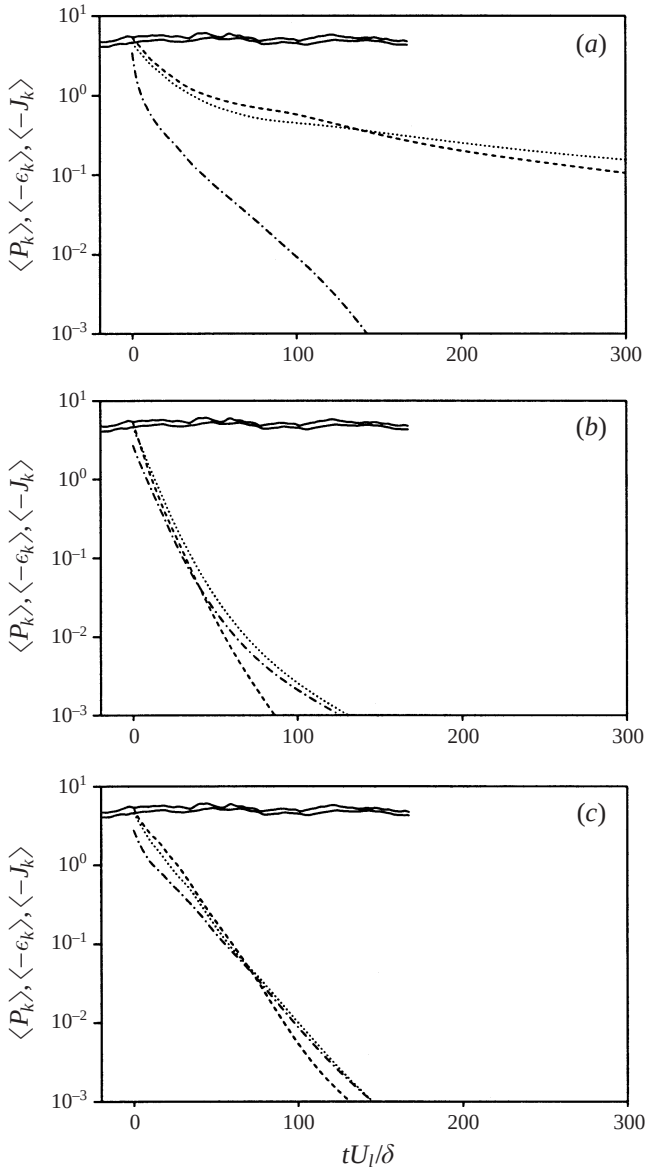

FIGURE 11. Time histories of the volume-averaged production ($\langle P_k\rangle$; - - - - -), viscous dissipation ($\langle -\epsilon_k\rangle$; · · · · · ·) and Joule dissipation ($\langle -J_k\rangle$; — • —) normalized by $u_{\tau o}^3/\delta$: (*a*) $N_x = 0.6$; (*b*) $N_y = 0.1$; (*c*) $N_z = 0.1$. The solid lines denote the volume-averaged production and viscous dissipation without magnetic field. Here, $\langle \bullet \rangle = (1/V) \int \bullet \, \mathrm{d}V$.

field, the streamwise and wall-normal vorticity fluctuation components are elongated in the wall-normal direction, and this feature is clearly discernible in the contour plot of the streamwise vorticity fluctuations in a crossflow plane. On the other hand, the iso-surfaces of the spanwise vorticity fluctuations do not clearly reveal this elongation (figure 12*c*), because the absolute magnitude of ω_z' near the wall is much greater than that of ω_z' in the channel-centre region owing to the formation of a thin Hartmann layer at the non-conducting wall. As Sommeria & Moreau (1982) considered, ω_z' in the

(*a*)

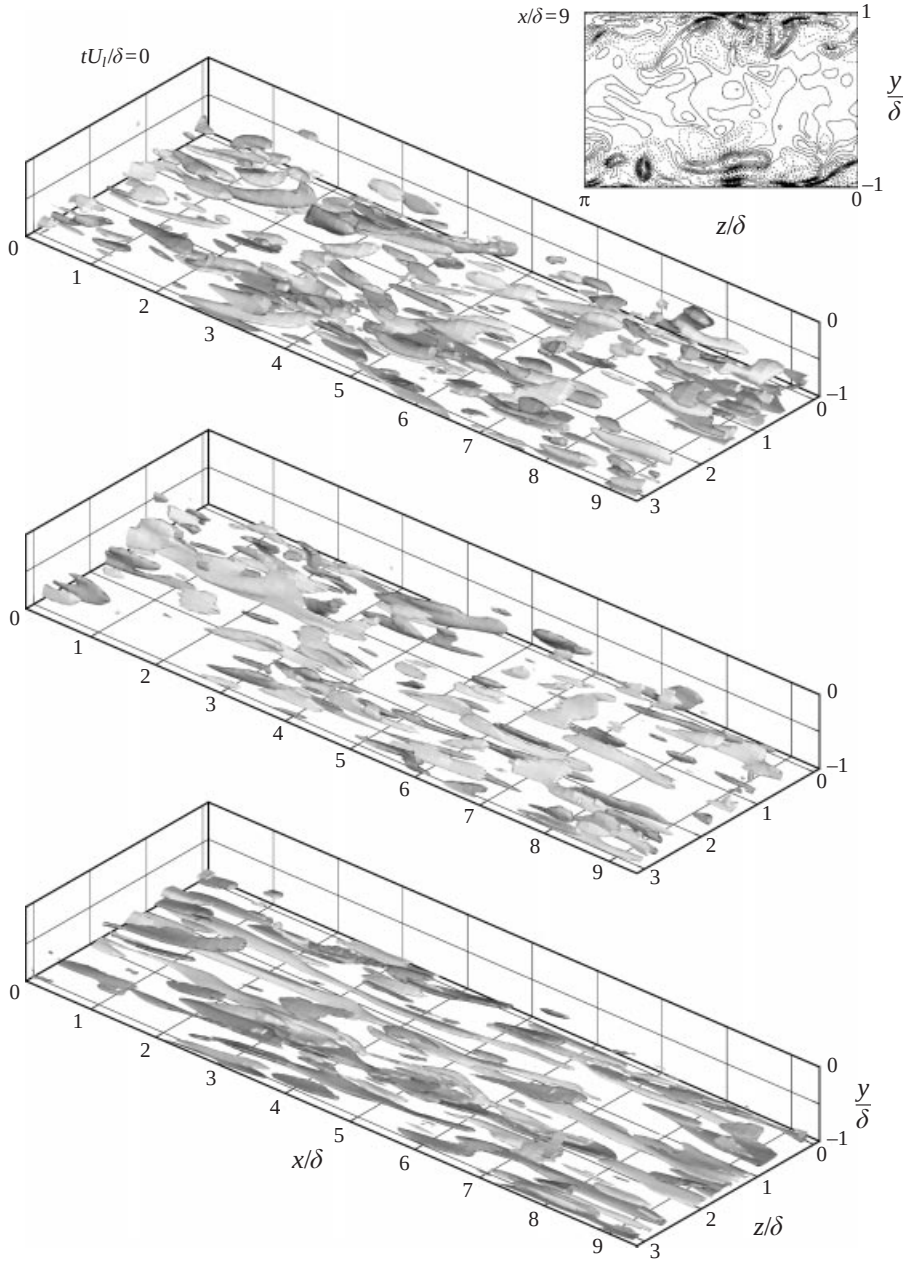

FIGURE 12(*a*). For caption see page 389.

channel-centre region is elongated along the wall-normal magnetic field (not shown here). The elongation of the vortical structures along the direction of the magnetic field was theoretically studied by Davidson (1995, 1997) as mentioned before in this paper.

Lumley & Newman (1977) identified a turbulence state in terms of the second (II)

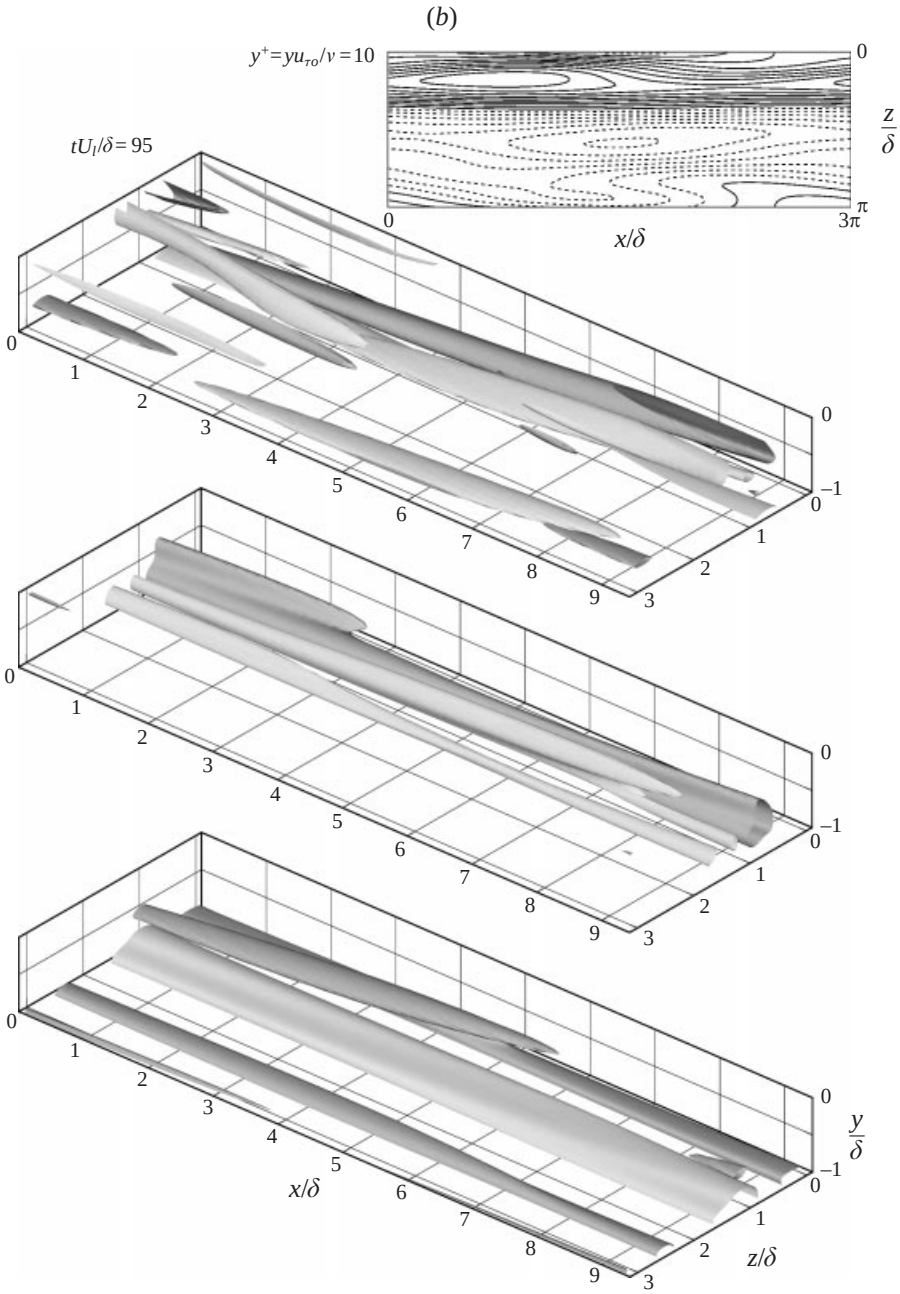

FIGURE 12(*b*). For caption see page 389.

and third (III) invariants of the Reynolds stress anisotropy tensor (b_{ij}), defined by

$$b_{ij} = \frac{\overline{u_i' u_j'}}{2\bar{k}} - \tfrac{1}{3}\delta_{ij}, \tag{5.2}$$

where δ_{ij} is the Kronecker delta tensor. The second and third invariants of b_{ij} are

(*c*)

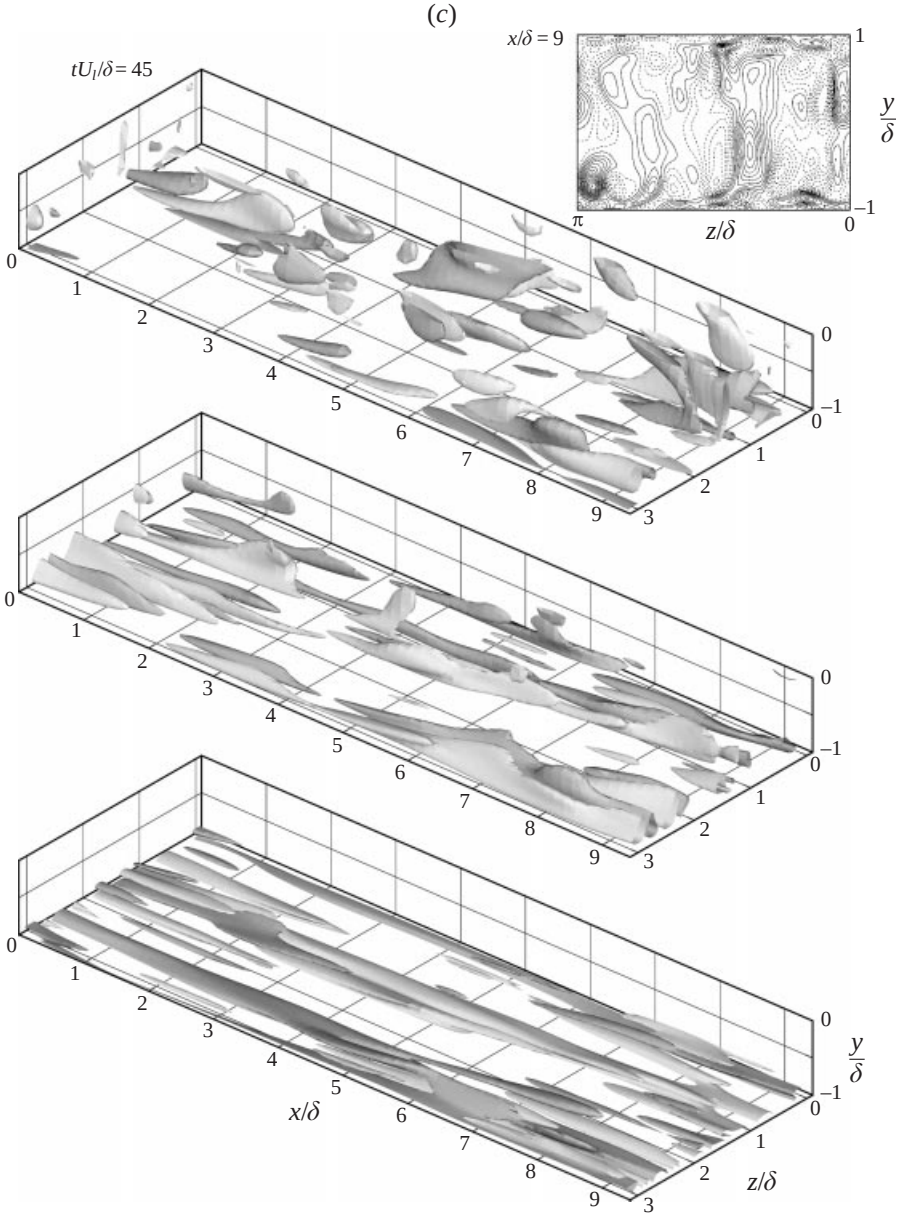

FIGURE 12(*c*). For caption see page 389.

given by

$$\mathrm{II} = -\tfrac{1}{2} b_{ij} b_{ji}, \tag{5.3}$$

$$\mathrm{III} = -\tfrac{1}{3} b_{ij} b_{jk} b_{ki}. \tag{5.4}$$

Turbulence states can be identified on a plot of $-\mathrm{II}$ *vs.* III. The anisotropy tensor for the vorticity is denoted by c_{ij}:

$$c_{ij} = \frac{\overline{\omega_i' \omega_j'}}{\overline{\omega^2}} - \tfrac{1}{3}\delta_{ij}, \tag{5.5}$$

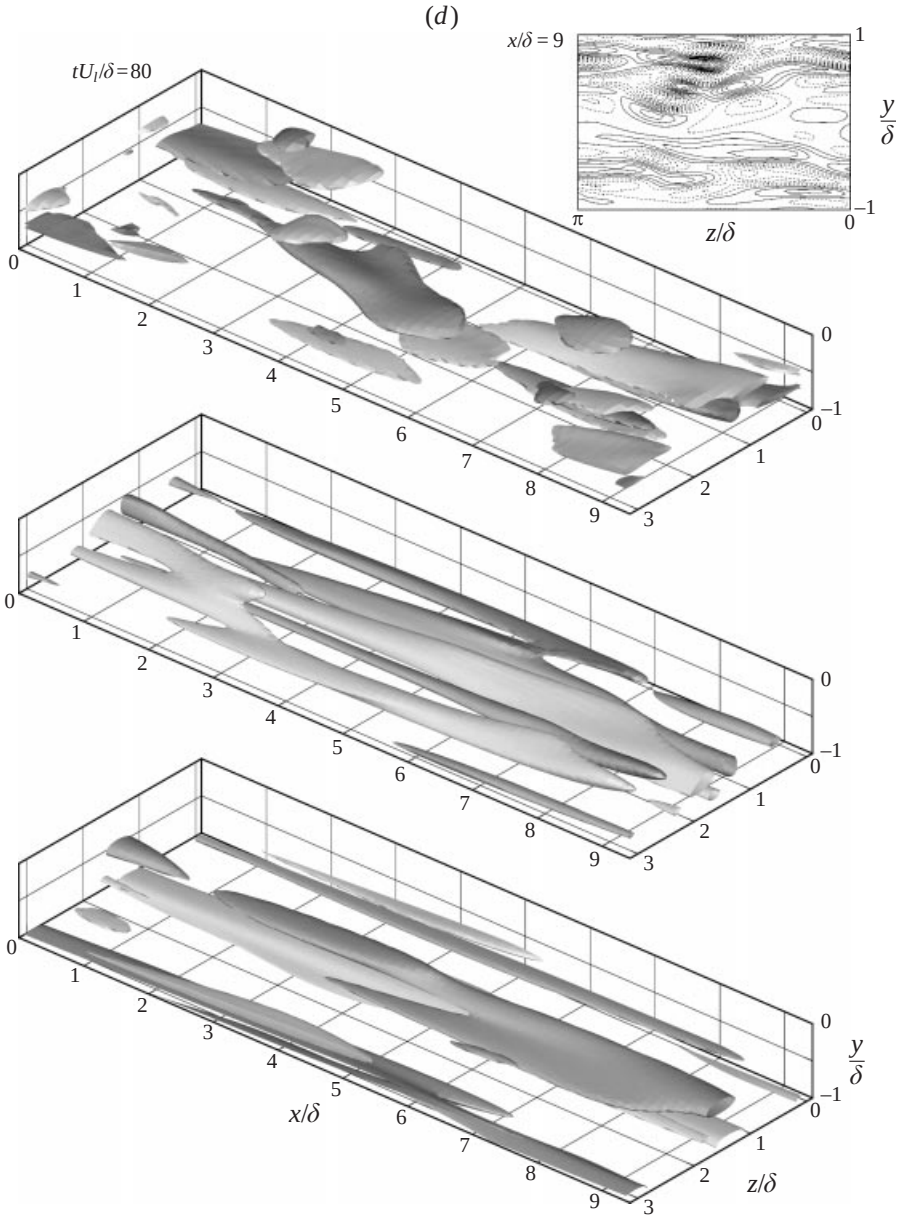

FIGURE 12. Iso-surfaces of the vorticity fluctuation components (streamwise, wall-normal and spanwise vorticity fluctuation components from top to bottom): (*a*) no magnetic field, iso-surfaces of $\omega_x\delta/u_{\tau o} = \pm 26$, $\omega_y\delta/u_{\tau o} = \pm 35$, $\omega_z\delta/u_{\tau o} = \pm 50$; (*b*) $N_x = 0.6$, iso-surfaces of $\omega_x = \pm 0.6$, $\omega_y = \pm 7$, $\omega_z = \pm 8$; (*c*) $N_y = 0.1$, iso-surfaces of $\omega_x = \pm 2.8$, $\omega_y = \pm 5$, $\omega_z = \pm 7$; (*d*) $N_z = 0.1$, iso-surfaces of $\omega_x = \pm 1.2$, $\omega_y = \pm 1.5$, $\omega_z = \pm 4$. Magnetic fields are applied at $t \geqslant 0$. Contours of ω_x are also plotted on the top right-hand corner to show the elongation of the structures.

where $\overline{\omega^2} = \overline{\omega_i'\omega_i'}$. The second and third invariants of c_{ij} can be similarly defined as those of b_{ij}. Owing to the properties of b_{ij} and c_{ij}, turbulence states are limited inside the region bounded by the two-component state and two axisymmetric states. Reynolds (1989) emphasized that, whereas b_{ij} contains information about the

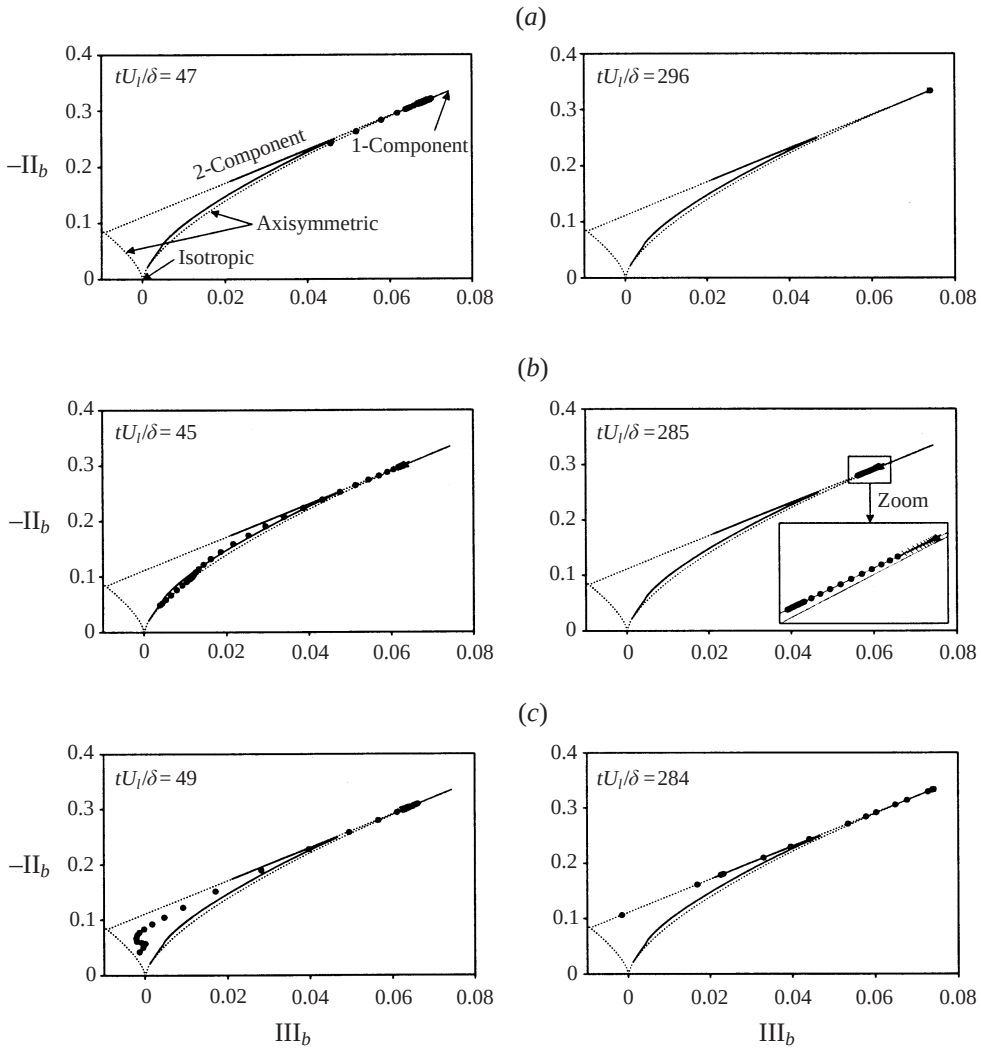

FIGURE 13. Time sequences of the anisotropy invariant map for the Reynolds stress tensor: (*a*) $N_x = 0.6$; (*b*) $N_y = 0.1$; (*c*) $N_z = 0.1$. ——, Without magnetic field; ×, $0 < y^+ \leqslant 10$ with magnetic field; ●, $10 < y^+ < 135$ with magnetic field. Magnetic fields are applied at $t \geqslant 0$. Here, $y^+ = yu_{\tau o}/v$.

'componentality', it does not contain any information about the 'dimensionality' of turbulence. However, when we study both b_{ij} and c_{ij} carefully, we may have some information on the dimensionality as well as the componentality in the case where the turbulence approaches the one-component state.

Figures 13 and 14 show, respectively, the time sequences of the anisotropy invariant maps (AIM) for b_{ij} and c_{ij} in the cases of strong magnetic fields. In the channel without magnetic field, the b_{ij} tensor varies from a two-component state near the wall to the nearly isotropic state in the centre of the channel, which is in good agreement with the computed result of Antonia, Kim & Browne (1991). With a strong streamwise magnetic field, the flow becomes one-component turbulence at all y-locations after a certain amount of transient time (figure 13*a*), which was also clearly shown in

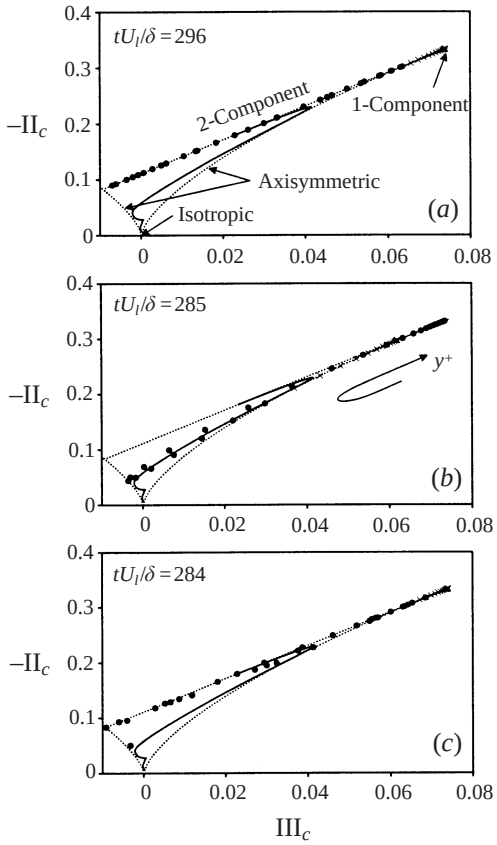

FIGURE 14. Anisotropy invariant map for the vorticity: (*a*) $N_x = 0.6$; (*b*) $N_y = 0.1$; (*c*) $N_z = 0.1$. ———, Without magnetic field; ×, $0 < y^+ \leqslant 10$ with magnetic field; ●, $10 < y^+ < 135$ with magnetic field. Magnetic fields are applied at $t \geqslant 0$. Here, $y^+ = yu_{\tau o}/\nu$.

figure 9(*a*), and the vorticity has nearly two-component characteristics (figure 14*a*), meaning that flow states approach one-component and two-dimensional turbulence. This is also consistent with the existence of the streamwise velocity fluctuations and the wall-normal and spanwise vorticity fluctuations after a considerable amount of time (figure 9*a*) and the elongation of turbulence structures in the streamwise direction (figure 12*b*).

With a strong wall-normal magnetic field, the flow becomes two-component (u and w) turbulence (figure 13*b*), and the vorticity in the channel-centre region becomes one-component (ω_y') turbulence (figure 14*b*) because the turbulence structures in the channel-centre region are elongated in the wall-normal direction. Then, we can conclude that $u' \approx u'(x, z)$ and $w' \approx w'(x, z)$ (that is, two-dimensional and two-component turbulence) in the channel-centre region, because $\omega_x' \approx \omega_z' \approx 0$, $v \approx 0$ and $\omega_y' \neq 0$ there.

With a strong spanwise magnetic field, the AIM near the wall becomes close to one-component (u') turbulence, and that in the other region characterizes two-component (u' and w') turbulence (figure 13*c*). The vorticity is close to two-component (ω_x' and ω_z') turbulence except for the flow state of one-component (ω_z') turbulence near the wall (figure 14*c*). Therefore, near the wall, $u = u(x, y)$.

6. Summary and discussion

Effects of the Lorentz force on near-wall turbulence structures were investigated using the direct numerical simulation technique with the assumption of no induced magnetic field at low magnetic Reynolds number. A uniform magnetic field was applied in the streamwise, wall-normal or spanwise direction to a turbulent channel flow with non-conducting walls.

The Lorentz force induced from the applied magnetic field reduced the intensity of the wall-layer structures. The skin friction decreased with increasing streamwise and spanwise magnetic fields, whereas it increased when the strength of the wall-normal magnetic field exceeded a certain value, because the drag increase due to the Hartmann effect was greater than the drag reduction due to turbulence suppression. All the turbulence intensities and Reynolds shear stress decreased with the wall-normal and spanwise magnetic fields, but the streamwise velocity fluctuations increased with the streamwise magnetic field although all other turbulence intensities decreased. It was also shown that the wall-normal magnetic field was much more effective than the streamwise and spanwise magnetic fields in reducing turbulent fluctuations, even though the wall-normal magnetic field interacted directly with the mean flow and resulted in drag increase at strong magnetic fields. It was also confirmed from the decrease of helicity fluctuations that the near-wall vortical structures in MHD channel flows become less helical.

All three components of root-mean-square current density fluctuations decreased with increasing magnetic fields owing to the decrease of the corresponding velocity and vorticity fluctuations. The production and viscous dissipation of the turbulent kinetic energy were significantly reduced by the applied magnetic field. It was also shown that the work performed by the Lorentz force fluctuations is nearly equal to the Joule dissipation near the channel centre, but very different near the wall, indicating the importance of the correlation between the electric potential and current density fluctuations near the wall.

In the channel with a strong streamwise magnetic field, two-dimensional streamwise velocity fluctuations $u = u(y, z)$ existed, even after other components of the velocity fluctuations and Reynolds shear stress nearly vanished. In the cases of strong wall-normal and spanwise magnetic fields, all the turbulence intensities, Reynolds shear stress and vorticity fluctuations decreased significantly and became zero. It was shown that the turbulence structures are markedly elongated in the direction of the applied magnetic field when it is strong enough. This observation is consistent with the theoretical investigation by Davidson (1995, 1997), who showed that flow structures should be elongated in the direction of the magnetic field in magnetic damping of jets and vortices because the Joule dissipation should be minimized to conserve the momentum. This argument has been confirmed in this study by investigating the time history of the volume-averaged Joule dissipation. The anisotropy invariant maps for the Reynolds stress and vorticity showed that there exists one-component and two-dimensional turbulence throughout the channel with a strong streamwise magnetic field, two-component and two-dimensional turbulence in the channel-centre region with a strong wall-normal magnetic field, and one-component and two-dimensional turbulence very near the wall with a strong spanwise magnetic field.

In §§ 4 and 5.1 (weak magnetic field), we have shown that the velocity and vorticity fluctuations are decreased by the magnetic field, and thus their integral scales are increased, but still smaller than the current computational domain size (see, for example, figure 7). At strong magnetic field (§ 5.2), however, the turbulence decays very rapidly and the flow becomes highly elongated in the direction of the applied

magnetic field. As a result, the lengthscales become very large at strong magnetic field. Therefore, a possible pollution of the results presented in § 5.2 might exist owing to the periodic boundary condition imposed in the streamwise and spanwise directions. In order to assess the effect of the periodic boundary condition on the results shown in §§ 4 and 5, we have performed simulations at weak and strong streamwise magnetic fields ($N_x = 0.2$ and 0.6, respectively) with twice the computational domain size (i.e. $L_x = 6\pi$ and $L_z = 2\pi$). The result showed that the drag, r.m.s. velocity and vorticity fluctuations, and their length scales are little affected by the current computational domain size at the Stuart numbers investigated in this paper.

We thank Professor John Kim at UCLA for the fruitful discussion at the initial stage of this work. The present work was supported by the Creative Research Initiatives of the Korean Ministry of Science and Technology. We greatly acknowledge the support.

REFERENCES

Alemany, A., Moreau, R., Sulem, P. L. & Frisch, U. 1979 Influence of an external magnetic field on homogeneous MHD turbulence. *J. Méc.* **18**, 277–313.

Antonia, R. A., Kim, J. & Browne, L. W. B. 1991 Some characteristics of small-scale turbulence in a turbulent duct flow. *J. Fluid Mech.* **233**, 369–388.

Branover, H. 1978 *Magnetohydrodynamic Flow in Ducts.* Halsted.

Brouillette, E. C. & Lykoudis, P. S. 1967 Magneto-fluid-mechanic channel flow. I. Experiment. *Phys. Fluids* **10**, 995–1002.

Choi, H., Lee, D., Lim, J. & Kim, J. 1997 Control of near-wall streamwise vortices using an electromagnetic force in a conducting fluid. *AIAA Paper* 97-2059.

Choi, H. & Moin, P. 1994 Effects of the computational time step on numerical solutions of turbulent flow. *J. Comput. Phys.* **113**, 1–4.

Choi, H., Moin, P. & Kim, J. 1992 Turbulent drag reduction: studies of feedback control & flow over riblets. *Rep. No.* TF-55. Department of Mechanical Engineering, Stanford University, Stanford, CA.

Choi, H., Moin, P. & Kim, J. 1993 Direct numerical simulation of turbulent flow over riblets. *J. Fluid Mech.* **255**, 503–539.

Choi, H., Moin, P. & Kim, J. 1994 Active turbulence control for drag reduction in wall-bounded flows. *J. Fluid Mech.* **262**, 75–110.

Davidson, P. A. 1995 Magnetic damping of jets and vortices. *J. Fluid Mech.* **299**, 153–186.

Davidson, P. A. 1997 The role of angular momentum in the magnetic damping of turbulence. *J. Fluid Mech.* **336**, 123–150.

Fraim, F. W. & Heiser, W. H. 1968 The effect of a strong longitudinal magnetic field on the flow of mercury in a circular tube. *J. Fluid Mech.* **33**, 397–413.

Gardner, R. A. & Lykoudis, P. S. 1971 Magneto-fluid-mechanic pipe flow in a transverse magnetic field. Part 1. Isothermal flow. *J. Fluid Mech.* **47**, 737–764.

Harris, L. P. 1960 *Hydromagnetic Channel Flows.* MIT Press/Wiley.

Hartmann, J. & Lazarus, F. 1937 Hg-Dynamics II. *Kgl. Danske Videnskab Selskab Mat.-Fys. Medd.* **15**, no. 7.

Hossain, M. 1991 Inverse energy cascades in three-dimensional turbulence. *Phys. Fluids* B **3**, 511–514.

Jeong, J. & Hussain, F. 1995 On the identification of a vortex. *J. Fluid Mech.* **285**, 69–94.

Kim, J. & Moin, P. 1985 Application of a fractional-step method to incompressible Navier–Stokes equations. *J. Comput. Phys.* **59**, 308–323.

Kim, J., Moin, P. & Moser, R. 1987 Turbulence statistics in fully developed channel flow at low Reynolds number. *J. Fluid Mech.* **177**, 133–166.

Kong, H., Choi, H. & Lee, J. S. 2000 Direct numerical simulation of turbulent thermal boundary layers. *Phys. Fluids* **12**, 2555–2568.

Krasilnikov, E. Y., Luschchik, V. G., Nikolaenko, V. S. & Panevin, I. G. 1971 Experimental

study of the flow of an electrically conducting liquid in a circular tube in an axial magnetic field. *Fluid Dyn.* **6**, 317–320.

Lee, D. & Choi, H. 2000 Direct numerical simulation of MHD turbulent flow in a channel. *Rep. No.* TFC-MS017. School of Mechanical and Aerospace Engineering, Seoul National University, Seoul, Korea.

Lim, J., Choi, H. & Kim, J. 1998 Control of streamwise vortices with uniform magnetic fluxes. *Phys. Fluids* **10**, 1997–2005.

Lumley, J. L. & Newman, G. R. 1977 The return to isotropy of homogeneous turbulence. *J. Fluid Mech.* **82**, 161–178.

Moffatt, H. K. 1978 *Magnetic Field Generation in Electrically Conducting Fluids*. Cambridge University Press.

Orlandi, P. 1996 Drag reduction in turbulent MHD pipe flows. In *Studying Turbulence Using Numerical Simulation Databases – VI, Proc. 1996 Summer Program of Center for Turbulence Research*, NASA-Ames Research Center and Stanford University, pp. 447–456.

Oughton, S., Priest, E. R. & Matthaeus, W. H. 1994 The influence of a mean magnetic field on three-dimensional magnetohydrodynamic turbulence. *J. Fluid Mech.* **280**, 95–117.

Reed, C. B. & Lykoudis, P. S. 1978 The effect of a transverse magnetic field on shear turbulence. *J. Fluid Mech.* **89**, 147–171.

Reynolds, W. C. 1989 Effects of rotation on homogeneous turbulence. *Proc. Tenth Australasian Fluid Mech. Conf.* (ed. A. E. Perry), KS2.1–KS2.6, University of Melbourne.

Shimomura, Y. 1991 Large eddy simulation of magnetohydrodynamic turbulent channel flows under a uniform magnetic field. *Phys. Fluids* A **3**, 3098–3106.

Sommeria, J. & Moreau, R. 1982 Why, how, and when, MHD turbulence becomes two-dimensional. *J. Fluid Mech.* **118**, 507–518.

Sureshkumar, R., Beris, A. N. & Handler, R. A. 1997 Direct numerical simulation of the turbulent channel flow of a polymer solution. *Phys. Fluids* **9**, 743–755.

Tsinober, A. 1990*a* MHD flow drag reduction. In *Viscous Drag Reduction in Boundary Layers* (ed. D. M. Bushnell & J. N. Hefner). AIAA Prog. Astron. Aeron. Series.

Tsinober, A. 1990*b* Turbulent drag reduction versus structure of turbulence. In *Structure of Turbulence and Drag Reduction* (ed. A. Gyr). Springer.

Walker, D. T. & Tiederman, W. G. 1990 Turbulent structure in a channel flow with polymer injection at the wall. *J. Fluid Mech.* **218**, 377–403.

Zikanov, O. & Thess, A. 1998 Direct numerical simulation of forced MHD turbulence at low magnetic Reynolds number. *J. Fluid Mech.* **358**, 299–333.